Chapter 4

Results

4.1 Morphological description

4.1.1 *Alouatta seniculus*

The *Alouatta seniculus* femora 25 544 l (Figures A.1, A.2) and 25 545 l (Figures A.3, A.4) belong to female individuals while 69.19 l (Figures A.5, A.6) is a femur of a male individual. The femoral heads of all specimens overtop slightly the greater trochanter. All of them have a roundish femoral head with a clear rim at the transition to the femoral neck. On the proximal side this rim flattens and fades towards the dorsum. On the dorsal side, the femoral head merges with the neck in an even transition. At the end of this transition an elongated bulge exists which is referred to as a small tuberculum and is displayed clearest on specimen 25 545 l ♀ (Figures A.7, A.8). The fovea capitis differs little between the samples. 25 544 l ♀ and 25 545 l ♀ both show flat, oval shaped foveas which are aligned in longitudinal direction. 69.19 l ♂ possesses a rounded, quite deep fovea capitis, which tapers of. A flat and semicircular area lies next to the fovea, extending sagittally. The oval shaped collum femoris demonstrates an angle of around 135.09° with the corpus according to the measurements listed in table 4.1 (individual data see Table B.26).

The fossa trochanterica has a narrow elliptic shape and is somewhat shallow in all specimens. 69.19 l ♂ has the deepest fossa trochanterica compared to 25 545 l ♀ and 25 544 l ♀. A linea trochanterica is absent in all specimens although a discrete crista intertrochanterica is commonly present. In 69.19 l ♂, this feature is displayed very well. The greater trochanter can be subdivided into three regions in all specimens. First, the superior part, shows a flat, slightly concave and pentagonal area. In 25 545 l ♀, a small, similarly shaped area adjoins this at the uppermost tip of the greater trochanter. These two areas are separated by a low border. The second region which all specimens have in common, comprises the anterior-lateral greater trochanter. This part is intensely structured by a uniform pattern with individual features. It extends anteriorly building a protuberance at the anterior tip of the greater trochanter and can

be seen best in 69.19 l ♂ and 25 545 l ♀. The disto-lateral area comprises the third region which all specimens have in common. It is made up of an even area in which a rudimentary tuberculum quadratum is present. 25 544 l ♀ shows this faint feature clearest of all specimens. Distally to this area extends a low tuberositas glutaea. The lesser trochanter extends anterio-medially. Its roughly triangular medial face pointing in distal direction is surrounded by a narrow rim. This rim is most prominent in 69.19 l ♂. At the distal edge of the triangular face a small linea pectinea originates. This line is only faintly developed in 25 545 l ♀ while the femur of 69.19 l ♂ shows it very well.

The corpus femoris is quite straight and only slightly curved anteriorly. The face of the shaft is uneven while the facies anterior is rather flat in all specimens. The posterior side is dominated by a pronounced labium laterale which originates at the tuberositas glutaea. It builds a prominent ridge and fades only a little bit in the lower third of the shaft. The quite even facies lateralis is only discernible in the upper third of the femur. A very faint line running from the inferior end of the linea pectinea towards the tuberculum adductorium can be identified as the labium mediale. Due to the faint labium mediale it is hard to recognize a facies medialis. The labiae do not merge resulting in the lack of a definite linea aspera. The area between both labiae is quite flat. A facies poplitea can therefore not be definitely observed, also.

A linea intercondylaris can only be noted on the specimen 69.19 l ♂. In the two other specimens, the area which should be the facies poplitea simply passes over into the fossa intercondylaris without any discontinuity. Specimen 69.19 l ♂ shows a quite uniform U-shaped fossa intercondylaris with gently rising sides towards the condyles. In 25 545 l ♀ and 25 544 l ♀ the fossa is clearly deeper and more asymmetric compared to 69.19 l ♂. The fossa also deepens definitely in its inferio-lateral part.

The condyles as well as a the broad U-shaped facies patellaris, in which the condyle areas merge, are bordered by a rim. This rim is rather low posteriorly and distally and becomes more narrow and prominent towards the anterior side. In 25 545 l ♀ and 25 544 l ♀, the condylus medialis protrude a bit more anteriorly compared to 69.19 l ♂. The condylus medialis becomes somewhat narrow towards its distal end, clearly displayed on 25 545 l ♀ and 25 544 l ♀. A tuberculum adductorium is very well defined and most prominent on 25 545 l ♀ forming a narrow border. The tuberculum adductorium emerges from the superior part of a well developed epicondylus medialis. Compared to the medial condylus, the condylus lateralis has a rather rounded contour. The sulcus popliteus is clearly present in all specimens as a deep elongated depression following the curvature of the lateral condyle. Above the condyles and the condylus lateralis, respectively, sesamoid bones are preserved in 69.19 l ♂ (Figure A.6) and 25 545 l ♀ (Figure A.4). Sesamoid bones were found in some specimens of *Presbytis entellus* and *Papio hamadryas*, as well.

4.1.2 *Presbytis entellus*

The *Presbytis entellus* femora used within this study comprises three articulated hind limbs (Figures A.9, A.10, A.11, A.12, A.13, and A.14) and a single femur (Figures A.15 and A.16). The description of the distal part of the articulated specimens as well as external morphometric measurements were hindered by the knee joint (Figure A.17). Unfortunately, no information about the sex of these specimens was available. The specimens 4745 l, 4746 l, and 4743 l exhibit unfused proximal epiphysis indicating that they are from subadult individuals. The distal epiphysis of specimen 4734 l shows a faint seam also, indicating a juvenile age. By default of adequate samples, these specimens had to be included although only adult individuals were meant to be investigated.

The caput femoris of *Presbytis entellus* has a hemispheric shape and is bordered by an edged rim. This rim flattens towards the dorsum and is sometimes (4734 l) extended distally. The fovea capitis, demonstrated by a flat, oval depression, extends sagittally and is surrounded by a shallow rim. Unlike *Alouatta seniculus* no tuberculum is present at the neck. *Presbytis entellus* has, as compared to the other specimens, a rather compact femoral neck. The fossa trochanterica deepens into a quite robust greater trochanter which overtops the caput femoris in all specimens. The superior portion of the greater trochanter is inclined medially and shows a deep depression proximo-anteriorly. Next to this depression a slightly structured area extends distally. Along the anterior side of the greater trochanter, a tuberosity is present which in the bigger specimens (4734 l, 4743 l) is displayed very well. The lower part of the greater trochanter merges seamless into the shaft. A tuberositas glutaea is absent in *Presbytis entellus*, but a faint tuberculum quadratum is present and is best visible in 4743 l and 4734 l. A linea intertrochanterica does not exist but from the medial edge of the greater trochanter a crista intertrochanterica arises. The lesser trochanter varies in shape with specimen. 4734 l has a rather rectangular trochanter minor, 4743 l shows a rather elongated one, and 4745 l has a narrow and quite elongated lesser trochanter while 4746 l exhibits a triangular shape. The medial face of the lesser trochanter is surrounded by a narrow rim. In 4745 l and 4746 l, this rim becomes clearly prominent anteriorly. A faint linea pectinea is visible on 4745 l.

The slightly convex corpus of the *Presbytis entellus* femora demonstrates an angle of approximately 135.49° with the collum. Only 4734 l shows an explicit convexity. The facies anterior is faintly rounded and in 4734 l quite even. The facies medialis is slightly rounded, while the facies lateralis is rather flat. The labium laterale originates on the inferior surface of the greater trochanter and becomes prominent in mid shaft but fades in the direction of the condylus lateralis. The upper third of the labium laterale is markedly textured on 4734 l. The labium mediale originates distal to the lesser trochanter. In mid shaft the labium mediale emerges less clearly compared to the labium laterale but it is definitely visible. The labium mediale fades distally towards the condylus medialis. A linea aspera is not present as both labiae do not converge. Instead a small groove is present between the labium mediale and laterale.

The facies poplitea is in all specimens rather inconspicuous and flat. The articulation of

the majority of the specimens hindered a detailed description. However, the slightly developed linea intercondylaris can be noticed on all specimens. The specimens 4743 l, 4745 l, and 4746 l show sesamoid bones above both condyles. The description of all further parts of the knee joint rely on the unarticulated specimen 4734 l. The fossa intercondylaris is relatively shallow and deepens just a bit distally. Both condyles are similar but the medial side is a bit more convex. A tuberculum adductorium is missing and the epicondylus medialis is just faintly pronounced. However, the epicondylus lateralis is quite prominent. The sulcus popliteus has a broad and flat shape. The facies patellaris is U-shaped and slightly inclined laterally. It is bordered laterally and medially by a rim which continues towards the posterior building the shallow margin of the condyles. This rim emerges explicitly at the superior end of the condyles.

4.1.3 *Papio hamadryas*

The *Papio hamadryas* sample shows quite striking sexual dimorphism in the femur size (female - 1.553 l, see Figures A.18, A.19 and males - Ha VIII 83 l, Ha VIII 3 l, and 3212 l, see Figures A.20, A.21, A.22, A.23, A.24, and A.25). The angle between shaft and neck of the *Papio hamadryas* femora shows an average inclination of 133.72°. The trochanter major clearly overtops the caput femoris in all specimens. The caput femoris is hemispheric in shape and is confined to the femoral neck by a narrow salient rim. In all specimens expect on 3212 l ♂, this rim flattens distinctly on the posterior. The fovea capitis has an elliptical shape, is elongated sagittally, and is bordered by a quite low rim. On the posterior surface of the femoral head next to the lateral rim, an oblong bulge lies adjacent to the fossa trochanterica. It resembles the tuberculum described at the identical position of *Alouatta seniculus* but is more prominent especially on the male specimens of *Papio hamadryas* (Figures A.26, A.27, A.28).

The fossa trochanterica of *Papio hamadryas* is quite broad and shallow compared to the rest of the sample group. It has an oval shape and deepens markedly into the greater trochanter in the male specimens. The lateral side of the greater trochanter is uniformly, and intensely structured especially in the male specimens. (Figures A.29, A.30). The superior tip of the greater trochanter shows varying textures and is always set off from the rest of the trochanter. On Ha VIII 3 l ♂ and 3212 l ♂, this tip is separated from the inferior area by a low rim while on Ha VIII 83 l ♂ and 1.553 l ♀, a faint but distinct curvature is present instead of a rim. Distally of this structure, an inward bowed area is present. This bowed ares is rectangular (3212 l ♂) or somewhat crescent shaped (Ha VIII 83 l ♂, Ha VIII 3 l ♂), opens distally and tilts anteriorly. Towards the anterior and distal parts, this area is bordered by a ridge which becomes quite prominent in the male specimens. Distally to the former mentioned area a triangular shaped plain is present, with one corner pointing towards the anterior side. This plain opens towards the posterior side and is distally bordered by a rim. On 3212 l ♂ an intensively structured ridge borders this plain posteriorly. Next to this plain, in the inferior most part of the greater trochanter another quite flat area is present. A large protuberance adjoins this area anteriorly, extending along the femoral neck towards the caput and creating a low but distinct ridge. This

protuberance phases out distally forming one prominent (3212 l ♂) or two shallow, parallel running ridges (Ha VIII 3 l ♂, Ha VIII 83 l ♂, 1.553 l ♀). The distal area of the trochanter major is bordered posteriorly by two faint ridges enclosing a narrow depression (Ha VIII 83 l ♂, Ha VIII 3 l ♂) or as one low ridge (1.553 l ♀, 3212 l ♂). Ha VIII 3 l ♂ shows a rising next to the former mentioned ridges but its designation as tuberculum quadratum seems questionable.

While a linea intertrochanterica is not present, a prominent crista intertrochanterica is formed by the inferior part of the greater trochanter. The lesser trochanter protrudes clearly, is quite slender and its medial face is bordered by two narrow rims. On 1.553 l ♀, 3212 l ♂, and Ha VIII 3 l ♂ a shallow border extends from the superior end of the two medial rims along the femoral neck. The lateral rim of 3212 l ♂ is textured and fused with the crista intertrochanterica. The linea pectinea is, in all specimens, formed by a narrow border. In the male specimens, the linea pectinea seems to be linked to the beginning of the labium mediale. The labium medial is developed as a shallow roughness superiorly. The labium laterale arises from the inferior extension of the greater trochanter. In 3212 l ♂ and Ha VIII 83 l ♂, a definite roughness is shown on the proximal part of the labium laterale indicating a tuberositas glutaea. The laterale and mediale labiae merge mid shaft, forming a clear linea aspera. Towards the inferior, both labiae part again creating the medial and lateral border of the facies poplitea. The corpus femoris itself has a convex curvature. Its anterior side is rather flat as well as the facies lateralis and medialis.

The facies poplitea is flat and separated from the fossa intercondylaris by a broad, low linea intercondylaris. While the fossa intercondylaris is quite shallow in the female individual (1.553 l ♀), it deepens in the males distally. The condylus medialis is broad compared to the lateral condylus. Only Ha VIII 83 l ♂ shows a clear tuberculum adductorium on a slightly protruding epicondylus medialis. On 3212 l ♂, the region proximal to the condyles is hindered by two sesamoid bones superior to the condyles. Another sesamoid bone is present above the lateral condylus of specimen 1.553 l ♀. These sesamoid bones are fixed to the specimens by dried connective tissue. The epicondylus lateralis is rather more prominent than the medial. The adjoining sulcus popliteus is broad and shallow. On 1.553 l ♀, the U-shaped facies patellaris is slightly inclined laterally. A narrow rim borders the facies patellaris and the condyles. This rim flattens near the condyles and protrudes again around the facies patellaris.

4.1.4 *Hylobates syndactylus / lar moloch*

Although they belong to different species, the specimens of *Hylobates syndactylus* (6983 l ♂, 52.36. l ♀) (Figures A.31, A.32, A.33, and A.34) and *Hylobates lar moloch* (47 979 r ♂) (Figures A.35, A.36) are quite similar in outer bone morphology. A spherical caput femoris overtops the greater trochanter on all specimens. The fovea capitis is shown as a fairly deep depression with its contours varying between an oval (47 979 r ♂ and 6983 l ♂) and elliptical shape (52.36. l ♀). Regardless of its form, the fovea capitis is always aligned sagittally. While it is developed as a crater-like pit in the smaller specimen of *Hylobates lar moloch* (47 979 r ♂), its dimensions

increase in *Hylobates syndactylus* (6983 l ♂, 52.36. l ♀). The fovea capitis spans the cortical bone and reveals parts of the cancellous bone. The femoral head in all specimens is bordered by a shallow rim with an uneven but similar course. On the medial side, this rim is recessed towards the caput creating an angular (47 979 r ♂, 6983 l ♂) or somewhat roundish (52.36. l ♀) indentation. Posteriorly this rim extends towards the femoral neck while anteriorly it becomes recessed.

The collum femoris has an elliptical contour and creates an angle with the shaft axis of 140.99° in *Hylobates lar moloch* (47 979 r ♂) and an average of 143.99° for two *Hylobates syndactylus* specimens. On the posterior side of the femoral neck, *Hylobates lar moloch* (47 979 r ♂) shows a narrow and shallow ridge which extends proximally (Figure A.37). This ridge could possibly be a rudimentary tuberculum as seen on *Alouatta seniculus* (for example 25 545 l ♀, Figure A.7) and *Papio hamadryas* (for example Ha VIII 3 l ♂, Figure A.28). The *Hylobates syndactylus* (6983 l ♂, 52.36. l ♀) specimens lack this feature. The fossa trochanterica has quite similar dimensions on both species despite the fact that the femur of *Hylobates lar moloch* (47 979 r ♂) is a bit smaller than that of *Hylobates syndactylus* (6983 l ♂, 52.36. l ♀). The fossa has an oval contour which is markedly deeper on the male individuals (47 979 r ♂ and 6983 l ♂) when compared to the female femur (52.36. l ♀). However, on all specimens, the fossa deepens through the cortex and reveals cancellous bone. The morphological features of the greater trochanter are quite similar in both species. On the superior area, a slightly concave area is presented and is bordered by a shallow rim. Towards the anterior, an area with a low structure is displayed. However, on the lateral and proximo-medial ends of this area, protuberances aligned longitudinally are present. These features are rather prominent in *Hylobates syndactylus* (6983 l ♂, 52.36. l ♀) (Figure A.38). On *Hylobates lar moloch* (47 979 r ♂), the proximal protuberance is low and roundish. The posterior area of the greater trochanter is flat and without a tuberculum quadratum. The anterior of the greater trochanter merges distally into a shallow tuberositas glutaea which is best developed in *Hylobates lar moloch* (47 979 r ♂).

While a linea intertrochanterica is absent, a faint crista intertrochanterica is present and merges into the posterior rim of the lesser trochanter. The lesser trochanter has a smooth oval face and is bordered by a low brim on the posterior and anterior sides. On *Hylobates lar moloch* (47 979 r ♂), the lesser trochanter is broader and less elongated compared to *Hylobates syndactylus* (6983 l ♂, 52.36. l ♀). Towards the shaft, a very faint linea pectinea is present. The corpus femoris is straight with a roundish shape. The facies anterior is dominated by this round shape in *Hylobates lar moloch* (47 979 r ♂) while the facies anterior of *Hylobates seniculus* (6983 l ♂, 52.36. l ♀) is broad and flat. Posteriorly only a faint labium laterale and labium mediale are present. Only on *Hylobates lar moloch* (47 979 r ♂) is the labium laterale slightly more pronounced. The facies lateralis steeply passes over to the facies anterior while the facies medialis forms a convex surface. As both labiae do not merge, no linea aspera can be defined.

Both *Hylobates syndactylus* (6983 l ♂, 52.36. l ♀) specimens show an even facies poplitea between the faint labiae. The *Hylobates lar moloch* sample (47 979 r ♂) presents a slightly

curved but quite uniform region causing the shaft to merge over into the fossa intercondylaris. A definite linea intercondylaris can not be noticed on all specimens. The fossa intercondylaris is broad, uniform and deepens distally. On the biggest specimen 52.36. l ♀ this depression is less intense and the fossa is broader. Both condyles are well rounded. The condylus medialis is bigger and has a broader articulation area compared to the lateral condylus. This difference between the condyles can be seen best on 47 979 r ♂ and 6983 l ♂. A tuberculum adductorium cannot be recognized. The epicondylus medialis is rather faint. Only on 52.36. l ♀ it is a bit more pronounced. The epicondylus lateralis is more prominent compared to the medial. The sulcus popliteus is broad and shallow and is deepest inferiorly. On 6983 l ♂ the sulcus is markedly even and rather shallow compared to the other specimens. The broad facies patellaris is inclined laterally. The rim bordering the facies patellaris and the articulation area of the condyles on *Hylobates syndactylus* (6983 l ♂ and 52.36. l ♀) is low. Only on the anterior side of *Hylobates lar moloch* (47 979 r ♂) does this rim become rather prominent.

4.1.5 *Homo sapiens*

Beside *Papio hamadryas* the size differences between male (11 l, 21 l) (Figures A.39, A.40, A.41, A.42) and female (10 l, 22 l) (Figures A.43, A.44, A.45, A.46) individuals in this sample are most striking. However, the characteristics under consideration are unaffected by this dimorphism. The femoral head has a spherical form and overtops the greater trochanter. Compared to the non-human primate sample, all *Homo sapiens* specimens have a rather shallow fovea capitis which is oval in outline with its longest axis roughly in sagittal direction. The fovea of 21 l ♂ is quite large compared to the other specimens and is surrounded by a bulging rim. Only on 22 l ♀ is this rim quite low. The boundary between the femoral head and neck is somewhat irregular and marked by a flat rim. This boundary extends onto the femoral neck posteriorly. The collum femoris has an elliptical profile. While the non-human specimens often show a tuberculum on the posterior surface, most of the human specimens (11 l ♂, 21 l ♂, 22 l ♀) demonstrate a protuberance anteriorly near the caput-collum boundary. On 21 l ♂ it is seen as a raised ridge which follows the caput-collum boundary, while on 11 l ♂ it is seen as a rough crescent band extending in transverse direction. Specimen 22 l ♀ shows an elongated knob aligned longitudinally. The angle between corpus and collum femoris is on average 136.98°.

The fossa trochanterica is oval in shape and in relation to the non-human primate specimens, quite shallow. While the fossa of 22 l ♀ only vaguely developed, 21 l ♂ exhibits the deepest fossa trochanterica of this group. As with the previous specimens the trochanter major can be subdivided into three regions (see Figure A.47). First, a triangular shaped superior area including the proximal edge of the greater trochanter. This area reaches with one point nearly towards the distal end of the greater trochanter. This triangle is more (21 l ♂) or less (10 l ♀) intensely structured and bordered by a rim. The second region, extending over the anterior of the greater trochanter has a crescent shape and a smooth structure. Towards the corpus femoris it is defined by a ridge. This ridge is seen clearly on 21 l ♂. The third region is defined as an

even triangular area on the posterio-lateral side with its base opening towards the posterior. On the distal surface it is limited by a rim. The rims of the three regions converge distally forming a protuberance.

A tuberculum quadratum is not recognizable on 10 l ♀, while 11 l ♂ and 22 l ♀ show it faintly, and 21 l ♂ exhibits it quite explicitly. Below the tuberculum quadratum the linea intertrochanterica begins and is a prominent, rough ridge superiorly. On female individuals (10 l ♀, 22 l ♀), the superior area is more raised when compared to the male individuals (11 l ♂, 21 l ♂). Inferiorly the linea intertrochanterica declines and becomes rough on 11 l ♂. The crista intertrochanterica is commonly formed by a broad bulge. The lesser trochanter protrudes faintly compared to the non-human primate specimens. Its oval face is limited proximo-laterally by a shallow rim and medially by a clear ridge but these borders are absent on 10 l ♀. The linea pectinea is developed variably. It is faint and narrow on 11 l ♂ but formes a clear ridge with a superior protuberance on 22 l ♀. On 10 l ♀, the linea pectinea is formed by a broad, flat rim. Specimen 21 l ♂ shows a shallow roughness distal to the lesser trochanter which is directed disto-laterally and could represent a special form of this feature.

The corpus femoris is somewhat convex and has a nearly triangular profile with rounded edges. The facies anterior is slightly curved. Although all specimens lack a definite tuberositas glutaea, the superior part of the labium laterale shows a distinct roughness. This resembles a tuberositas glutaea but the feature is positioned much more medially than expected. While on 10 l ♀ and 22 l ♀ the labium laterale fades a bit distally, 11 l ♂ and 21 l ♂ show a definite narrow rim. The linea intertrochanterica continues as the labium mediale. The transition zone across the facies medialis and superior part of the labium mediale is on 11 l ♂ and 21 l ♂ developed as a rough rim, while it is formed as a shallow rim on 10 l ♀ and 22 l ♀. Inferiorly it adjoins the tuberculum adductorium which is demonstrated as a knob. Only 21 l ♂ shows a prominent rough ridge instead. Both facies lateralis and facies medialis are fairly even. The facies lateralis forms a steep surface while the facies medialis is less angled. The linea aspera is seen as a prominent more (11 l ♂, 21 l ♂) or less (10 l ♀) rough ridge. Only 22 l ♀ lacks this roughness showing instead a fairly homogeneous, roundish ridge.

The facies poplitea is quite flat and on 10 l ♀ and 22 l ♀ slightly concave. In its disto-medial part, a definite elevation is noticeable. A broad strip defines the linea intercondylaris which is extraordinarily low on 21 l ♂. The adjoining fossa intercondylaris is flat and deepens inferiorly, especially on 22 l ♀. Compared to the non-human specimens, both condyles are quite similarly shaped. The epicondylus lateralis and especially the epicondylus medialis are far less prominent in these specimens than the non-human samples. The sulcus popliteus is quite faintly developed and forms a very shallow trench running parallel towards the course of the condylus lateralis. The facies patellaris is formed by a lateral inclined U-shaped from. It is bordered by a low rim, which also forms the margin of the condyles. On 11 l ♂, this margin is bulging and sharply edged indicating arthrosis.

4.1.6 *Pliopithecus vindobonensis*

In the following, the right femur of individuum I (O.E. 304 r) (Figures A.48, A.49), two proximal fragments of left femora (O.E. 559 l and O.E. 560 l) (Figures A.50, A.51 and A.52, A.53), the right (1970/1397/22 r) and left (1970/1397/23 l) femur of individuum II (Figures A.54, A.55), and another proximal left femur fragment (1970/1398/2 l) (Figure A.56) are described. By first inspection it becomes obvious that the right femur of individuum II (1970/1397/22 r) is clearly bigger compared to the left one (1970/1397/23 l) (see B.27).

In all specimens the caput femoris overtops the trochanter major. Zapfe (1960) remarked that all these femora show epiphyseal boundaries in radiographs but only O.E. 560 l and 1970/1398/2 l show macroscopically clear unfused epiphyses. The epiphyseal boundaries, visible on the femora of individuum II (1970/1397/23 l and 1970/1397/22 r), seem to be quite fused when compared to O.E. 560 l and 1970/1398/2 l. The caput of all these specimens is roundish in form. The fovea capitis of O.E. 560 l is enlarged and deep when compared to the five other specimens. It forms of a rounded square containing two pits with the inferior pit being deeper than the superior. The pits are separated by a narrow rim which runs sagittally in a concave curve. In O.E. 304 r, the fovea capitis is teardrop shaped with an oval pit anteriorly which deepens intensely towards its center. The fovea of O.E. 559 l forms a trapezoid extending sagitally and with its maximum depth above the baseline of the trapezoid. The femur fragment 1970/1398/2 l shows a deep crescent fovea capitis which opens anterio-proximally. On both femora of individuum II (1970/1397/23 l, 1970/1397/22 r), the fovea capitis is present as a shallow, oval depression pointing anteriorly. The caput femoris is well separated from the collum femoris except on the posterior side. O.E. 304 r, O.E. 559 l and 1970/1398/2 l show a low ridge separating the caput from the beginning of the collum femoris. On the dorsal side, the caput femoris is recessed towards the collum. In this way a dent is formed in the homogeneous contour of the caput boundary and merges seamlessly with the collum. Instead of a dent the femora of individuum II show a remarkable boomerang shaped (1970/1397/23 l) and crescent shaped enlargement (1970/1397/22 r) at the caput/collum boundary.

The collum femoris of all specimens has an elliptical profile and branches from the corpus femoris at an angle of approximately 133.80° according to the measurements listed in 4.1 (individual data see B.27). Posteriorly on the collum next to the medial end of the fossa trochanterica, a tuberculum is present, which has already been mentioned by Zapfe 1960. The tuberculum can be seen clearly on 1970/1398/2 l. On O.E. 304 r, this tuberculum is slightly lower when compared to 1970/1398/2 l creating a longitudinally extended protuberance. 1970/1398/2 l shows a low ridge running proximo-lateral to disto-medially atop the tuberculum. O.E. 304 r shows a shallow depression, laterally above the tuberculum. This depression forms an isosceles triangle which points towards the tuberculum. The baseline of this triangle extends transversely between the collum and the trochanter major. The fragment 1970/1398/2 l lacks such a depression. On O.E. 559 l, the tuberculum is smoother and a shallow depression is located directly above it. This depression is roughly triangular with the deepest part pointing towards the col-

lum and a foramen located in it. O.E. 560 l shows a broad tuberculum which extends towards the collum. The depression located above it is trench-like in shape. It runs from the medial end of the fossa trochanterica towards the superior part of the caput-collum boundary and contains some irregular pits directly above the tuberculum which contain some foramina. The left femur of individuum II (1970/1397/23 l) shows only a very smooth tuberculum and a small, shallow lens-shaped depression lateral above it of questionable origin. On the right femur of the same individuum (1970/1397/22 r), the tuberculum is even less detectable but a very small, shallow, roughly triangular depression containing a medial foramen is present. Similar tuberculae were detected on *Alouatta seniculus*, *Papio hamadryas*, and *Hylobates lar moloch*.

All specimens lack a linea intertrochanterica while a crista intertrochanterica is developed on all and is most prominent in O.E. 560 l, O.E. 304 r, and 1970/1398/2 l. The crista intertrochanterica merges with a low posterior rim. This rim builds the medial face of the trochanter minor and is best seen on O.E. 304 r, O.E. 559 l, and 1970/1397/23 l. The medial facet of the trochanter minor is convex and elongated longitudinally. On O.E. 559 l, this facet is markedly more elongate when compared to the other specimens and creates a longitudinal extension of the lesser trochanter. On 1970/1397/23 l this facet divides into two halves with the posterior half having an oval shape and extending longitudinally. The anterior half is crescent shaped and opens posteriorly. At 1970/1398/2 l, this facet is seen less clearly due the structures on its surface. On O.E. 560 l the distal part of the lesser trochanter is absent. Therefore, it is not possible to determine the real extent and shape of the facet on this specimen even though it appears that the facet might have been narrower and longer compared to O.E. 559 l. Anteriorly the facet is bordered by a narrow ridge and is seen very well on specimens O.E. 304 r, O.E. 559 l, and 1970/1397/22 r. On O.E. 560 l, a part of this ridge is lacking due to diagenetic damage. The whole region where this ridge is presented and parts of the anterior facies of the lesser trochanter are destroyed on 1970/1398/2 l. Anteriorly on O.E 304 r, O.E. 559 l, O.E. 560 l, and 1970/1397/22 r, the trochanter minor is concavely shaped and is well defined on O.E. 304 r and O.E. 559 l. On O.E. 560 l, only the proximal area of the anterior trochanter minor shows a clear concave face. For 1970/1398/2 l, no such feature could be discerned due to diagenetic damage anteriorly on the lesser trochanter. 1970/1397/23 l shows no concaveness here at all. The trochanter minor is in all specimens aligned medio-posteriorly.

On all specimens a deep fossa trochanterica with an elliptic (O.E. 304 r, O.E. 560 l, 1970/1398/2 l) or a roundish contour (O.E. 559 l, 1970/1397/23 l, 1970/1397/22 r) is seen. The trochanter major on all specimens is intensely structured by an uniform pattern in its superior and anterio-lateral parts. It shows at its superio-lateral tip a shallow elliptic depression (O.E. 304 r, O.E. 559 l, 1970/1397/22 r) elongated sagittally and surrounded by a bulging rim which is most prominent on O.E. 304 r. Instead of this depression a facet is displayed on 1970/1398/2 l and 1970/1397/23 l, whereas on O.E. 560 l this area is not preserved due to diagenetic damage. Below this depression a crescent area is seen, opening proximally and surrounded by a bulging rim, which is very well seen on O.E. 560 l. At the disto-anterior end of this area, a tuberculum is present and has an oval form which is demonstrated very well on

O.E. 304 r, O.E. 559 l, and 1970/1397/23 l. On 1970/1397/22 r, the tuberculum is remarkably lesser prominent when compared to 1970/1397/23 l. This region is damaged on 1970/1398/2 l disabling any description. Below this tuberculum an oval (1970/1397/23 l) or crescent (O.E. 304 r, O.E. 559 l, O.E. 560 l, 1970/1397/22 r) depression opens anteriorly. This crescent depression is quite smooth on 1970/1398/2 l when compared to all other specimens. Its superior and anterior parts have a broad, prominent rim which becomes quite narrow latero-inferiorly. O.E. 559 l shows a narrow, accentuated last next to the anterior part of this rim. On O.E. 304 r, this last is present as well but is less defined from the rim than on O.E. 559 l. The latero-inferior area of the trochanter major is eroded on O.E. 560 l. Therefore, the rim of the previously mentioned depression is rounded with areas of its superior part missing. Due to the wear it is not clear if an adjoining last existed on this specimen too. On O.E. 304 r and O.E. 559 l, two small lasts run in a superiorly arcing line over the lateral side of the trochanter major. They originate on the medio-inferior end of the depression rim on the most inferior area of the greater trochanter. These lasts extend downward and join each other inferiorly on the trochanter major. Despite the eroded condition of this region on O.E. 560 l, there are indications of these two lasts. On 1970/1397/23 l, similar traces are seen. The fragment 1970/1398/2 l and the right femur of individuum II (1970/1397/22 r) are partly damaged at this region and no evidences of these lasts are recognizable.

The two conjoined lasts form a low ridge below the trochanter major. This ridge is the anterior border of a structured, elongate oval area indicating a rudimentary trochanter tertius. On the right femur (1970/1397/22 r) a rudimentary trochanter tertius is much more prominent when compared to the left femur (1970/1397/23 l). The fragment of O.E. 560 l lacks this region. Below the trochanter tertius a ridge emerges from the anterior border. It flattens and extends distally creating a very smooth labium laterale. A similar low ridge running inferiorly from the trochanter minor forms the labium mediale. On O.E. 304 r and the left femur of individuum II (1970/1397/23) l, the labium mediale creates a narrow ridge inferiorly on the facies poplitea. On the right femur of individuum II (1970/1397/22 r), a clear rim exists here as well but its curvature is not as sharp as on the former mentioned specimens. The labium laterale and the labium mediale slightly converge in the mid shaft region. A linea aspera, facies lateralis and facies medialis are not observable. The facies anterior is rounded. The area between the labium laterale and labium mediale is slightly rounded superiorly and flattens towards the facies poplitea. As mentioned by Zapfe (1960) the sagittally convexity of the very straight shafts of all complete Neudorf an der March femora may be due to glued joints. The reconstructions could have over straightened the shafts as well making definite statements about the shaft form of *Pliopithecus vindobonensis* impossible without a detailed investigation of the single fragments.

Due to the course of the labium laterale and mediale it is not possible to mark the beginning of the facies poplitea. O.E. 304 r, 1970/1397/23 l, and 1970/1397/22 r show a tuberosity on the medial side of the inferior facies poplitea. The linea intercondylaris of O.E. 304 r is present as a prominent ridge disconnected in the medio-lateral half. On the femora of individuum II (1970/1397/23 l, 1970/1397/22 r) the linea intercondylaris creates a broad, low ridge. The fossa

intercondylaris is deep and consists of two oval pits. These pits, one lying above the other, are separated by a high, narrow ridge, with the inferior pit being smaller than the superior. Towards the condyles and the facies patellaris a bulging rim creates the medial, distal and lateral border of the fossa intercondylaris. This rim is most prominent on O.E. 304 r especially at the condylus medialis. On 1970/1397/23 l and 1970/1397/22 r this rim is somewhat smoother and continues more slightly as superior, lateral, and medial border of the condyles. On 1970/1397/23 l and 1970/1397/22 r the rim vanishes superior of the condylus medialis. On the proximo-medial side of the condylus medialis of O.E. 304 r, a surface roughness is present and was interpreted by Drexler in Zapfe (1960) as a sign of a minor arthritic process. The rim of the condyles proceeds anteriorly as superior, lateral and medial border of the U-shaped facies patellaris. Both condyles are of relatively even size. The condylus medialis is more convex than the condylus lateralis. The lateral condylus is not uniformly curved, has a shallow depression proximo-medially which is most clearly shown on O.E. 304 r. The epicondylus medialis is smooth. A tuberculum adductorium is not present on O.E. 304 r whereas 1970/1397/23 l and 1970/1397/22 r clearly show this feature. The epicondylus lateralis is separated by a broad sulcus popliteus from the condylus lateralis and is developed as a prominent tuberosity.

4.1.7 *Paidopithex rhenanus*

The femur of *Paidopithex rhenanus* (Din 45 r) (Figures A.57, A.58) has been an object of controversy since the 19th century as described in chapter 2.2.2 (Dubois 1895, Pohlig 1895, Gieseler 1926, Begun 1992). Detailed descriptions of its external morphology were given by Zapfe (1960) and compared with the femora of *Pliopithecus vindobonensis* by Begun (1992).

The Eppelsheim femur is generally comparable in its overall appearance to the femora of *Pliopithecus vindobonensis*. The femoral head is nearly perfectly round and heavily pitted anterio-laterally by a deep fossa. An abrasion area adjoins the fossa distally. A minor abrasion is also present on a small region of the posterior caput-collum boundary. The clear division of caput and collum, mentioned by Zapfe (1960), can therefore not be confirmed. The femoral head is slightly higher in position than the greater trochanter. The fovea capitis is more pronounced here when compared to *Pliopithecus vindobonensis* and has an oval form which extends sagittally. The fovea is bordered proximo-anteriorly by a shallow depression. The fovea capitis itself is separated by a low last. In its proximo-anterior half, a conical pit is present and in its posterio-distal half a deep crescent depression, opening anterio-proximally, is seen. In the proximal area of this lower half a single, deep conical pit is present. In the inferior area of the lower half, three smaller, shallower pits exist. The rim of the fovea capitis shows signs that it may has been subjected to abrasion.

Posteriorly the articular surface of the caput extends towards the collum. This extension is separated from the neck by a flat rim. Between the extension and the trochanteric fossa, a tuberculum similar that of *Pliopithecus vindobonensis* is present (Figure A.59). The tuberculum is an

oblong protuberance extending longitudinally. The latero-distal area of the tuberculum is damaged by a groove running obliquely from superio-lateral to the inferio-medial part. Therefore, the exact shape of the tuberculum can not be described. A depression above the tuberculum, comparable to that of *Pliopithecus vindobonensis*, is not visible. However, a foramen inserts medially above the tuberculum in the neck. The collum has an oblong elliptic profile, its anterior and posterior sides are quite even and it creates an angle of 138.99° with the femoral shaft.

The fossa trochanterica is roundish in contour and can be separated into two parts. The anterior area is elliptical in form and reaches very deep into the greater trochanter while the posterior area forms a less deep oval foveola. The trochanter major is prominent and orients slightly to the anterior and is anterio-laterally structured like on *Pliopithecus vindobonensis*. A shallow elliptic depression is present at its proximo-lateral tip. The depression extends sagittally and is surrounded by a bulging rim. At the inferior end of the greater trochanter a smooth oval depression facing latero-anteriorly can be seen. This depression is surrounded by a flat rim, which becomes prominent by forming the superior and lateral boundary of the depression. The other structures described on the greater trochanter of *Pliopithecus vindobonensis* are not presented on this specimen. Below the greater trochanter a glutaeal tuberosity extends longitudinally, indicating a rudimentary trochanter tertius comparable to *Pliopithecus vindobonensis*. A linea intertrochanterica is absent although a definite intertrochanteric crest can be seen like on *Pliopithecus vindobonensis*.

The lesser trochanter is aligned posterio-medially. Due to wear the major posterior part of the lesser trochanter is damaged, therefore, a statement about the insertion of the intertrochanteric crest in the lesser trochanter is impossible. It seems that the anterior rim of the medially directed surface of the lesser trochanter is build by a narrow last. This last seems to continue distally forming a linea pectinea. There might have been a connection between the pectineal line and the labium mediale but due to missing bone splinters and glued areas in this region such a connection can not be definitely stated. Superiorly the labium mediale is smooth and emerges towards the distal end forming a narrow, prominent rim on the medial border of the popliteal surface. The labium laterale extends from greater trochanter over the glutaeal tuberosity towards the lateral side of the facies poplitea. Proximally and in mid shaft the labium laterale emerges clearly, but declines inferiorly forming a less definite lateral boundary of the facies poplitea compared to the smooth labium mediale. A linea aspera is not displayed, as the medial and lateral labiae do not merge. The area between both labiae is slightly convex and flattens towards the facies poplitea, like on *Pliopithecus vindobonensis*. The shaft is rounded anteriorly and flattens laterally. However, the straight form of the shaft as well as the slightly anteriorly positioned femoral head and neck have to be interpreted carefully, as the reconstruction might have influenced these features.

Inferiorly the femur is more seriously damaged than proximally, especially on the lateral and medial side of the condyles, therefore, a less detailed description of there parts can be given. The medial condyle is roundish in contour, rather robust and slightly bigger than the lateral condyle.

Above the condylus medialis a very shallow tuberculum adductorium is present, which is joined laterally by an elliptic, shallow groove. The condylus lateralis is oblate in contour and laterally intensely structured. A strong epicondylus lateralis is displayed and separated from the lateral condyle by a slightly abraded sulcus popliteus. A distinct elliptic groove lies anterio-proximally to the epicondylus lateralis. The articular surfaces of the condyles join each other anteriorly in a broad, U-shaped facies patellaris. The intercondylaric line is seen as a smooth ridge. It runs two-thirds of the intercondylaric distance from the lateral to the medial condyle before it is cut by a longitudinal trench. The fossa intercondylaris is separated by a shallow foveola superiorly and a deeper oval pit inferiorly.

4.2 External Bone Morphometry

The individual results of the bone surface morphometrical description are listed in appendix B (Table B.1 - Table B.25). The species-pooled table 4.1 as well as the average data of individual specimens (Table B.26 and B.27) show the differences in the bone surface morphometry. It must be noted that parameter H could not be definitely determined on O.E. 560 l due to the absence of the major part of the shaft. The difference in parameters between specimens are caused by differences in body proportion, size, weight, and by differential loading conditions. These individual conditions are reflected in the bone surface morphometry. Thus the sample size is definitely too small to permit a reliable statistical evaluation. However, the gross morphological features of the seven species groups are displayed clearly.

Regarding these data another fact becomes obvious: each species belonging to a locomotionally distinct group demonstrates particular gross anatomical features. Therefore, no two species exist which have different locomotor preferences but same body sizes and proportions and makes a comparison of this data quite difficult. Since the bone surface morphometry is directly influenced by the attached muscles, tendons, and ligaments their qualities must be considered as well. Fischer (1961) and Gerhartz (1962) carried out studies on the hip and thigh muscles of *Papio leucophaeus* and *Ateles*, respectively. These detailed studies considered the functional aspect of the muscles but did not account for bone morphology.

In the beginning of the present study it was planned to carry out some incipient examinations of the thigh and hip muscles of primates. However, the realization of even preliminary investigations of muscle groups should be accomplished after an integrative procedure, ensuring an effective use of the rare material. Further, a standardized way to calibrate the data to exclude or reduce the influence of allometric differences must be developed, to enable reliable comparisons. Many factors beside the muscle proportions must be considered, such as the area and position of the muscle insertions and the quantity and quality of the fibre orientation of muscles, tendons, and ligaments. Unfortunately detailed dissections were beyond the scope of this work. However, this data demonstrates variability between the selected primate groups of the different features measured.

Table 4.1: The average pooled values of the extant species

	n	A [mm]	B [mm]	C [mm]	D [mm]	E [mm]	F [mm]	G_l [mm]	G_m [mm]	H [°]
Alouatta seniculus	3	156.31	26.06	24.82	13.39	9.59	31.77	22.50	25.70	135.09
Presbytis entellus	4	210.46	34.09	29.58	16.56	14.89	38.08			
(only 4734 l, 4745 l, 4746 l)	(1)									135.49
(only 4734 l)	(1)							(28.40)	(34.60)	
Papio hamadryas	4	225.34	43.46	34.04	19.79	15.01	45.78	31.03	38.10	133.72
Hylobates lar moloch	1	203.69	29.21	26.56	15.38	10.77	32.30	25.60	28.60	140.99
Hylobates seniculus	2	209.04	33.42	29.96	18.34	10.93	36.50	27.90	32.75	143.99
Homo sapiens	4	469.50	92.57	80.34	44.39	34.64	88.45	62.70	77.10	136.48
Pliopithecus vindobonensis	6		37.14		16.50	12.70				133.80
(only O.E. 304, 1970/1397/22, 1970/1397/23)	(3)	(209.30)		(32.04)				(31.07)	(32.95)	
(only O.E. 304, 1970/1397/22, 1970/1397/23,	(4)						(37.54)			
1970/1398/2)										
Paidopithex rhenanus (Din 45)	1	282.76	49.85	41.07	22.13	16.95	58.30	32.80	35.60	138.99

4.3 High resolution CT images and their histomorphometric data

4.3.1 High resolution CT images

High resolution CT images clearly display the different spatial arrangement of the cancellous bone. Characteristics of the different architectures are described below. The pictures of cancellous bone in this chapter were all taken from comparable positions in the 3D CT images. The gross trabecular architecture of the proximal femur was imaged by a sectional view running through the center of the femoral head and the greater trochanter. The view in the trabecular architecture of the lesser trochanter was obtained by a cutting plain positioned parallel to the direction of main extension of the lesser trochanter.

Alouatta seniculus

The proximal femur of *Alouatta seniculus* reveals a generally dispersed cancellous structure compared to other specimens. In the femoral head a rather homogenous structure is present. Two weakly developed preferred directions of alignment are visible in 69.19 l ♂ (Figure 4.1). Both of these trajectorial bundles can be distinguished from the adjoining cancellous bone by their plate-like elements, emphasizing the structures which run in the directions described below. One of these trajectorial bundles emerges from the inferior cortex of the neck fanning out upward under the same angle as the neck. It can be seen from the neck as far as the proximal third of the femoral head. This structure is not discernible in the most anterior areas. The plate-like trabeculae of this trajectory lie sub-parallel to the sagittal plain. The second, more faintly visible trajectorial structure originates from the superior cortex of the neck and also coursing into the femoral head. This structure emerges clearly near the mid part of the head but can be tracked only along a short distance. These plate-like trabeculae lie in an oblique plain extending in sagittal direction. In the lateral part of the femoral head, the second trajectorial sheaf weakly penetrates through the first. Around these two bundles, radially arranged trabeculae of plate-like or prolate shape are present. In 25 545 l ♀ and especially 25 544 l ♀, the first trajectorial structure is faintly displayed, while the second trajectorial structure is barely recognizable (Figures 4.2 and 4.3). Closer examination of the lateral side of the femoral head reveal an alignment of trabecular elements. They run like in 69.19 l ♂ in the same direction as the femoral neck and present a weak trajectorial structure. In the two female samples this structure continues laterally into the femoral neck and merges inferiorly with plate-like structures below the greater trochanter. 25 544 l ♀ shows this feature more clearly than 25 545 l ♀.

Regarding 69.19 l ♂ and 25 545 l ♀, the cancellous bone fades in the region of the femoral neck. Only few trabeculae are present and these are widely separated, loosely connected, and without a definite direction. In 25 544 l ♀, the trabeculae fade also but less explicitly than in the former specimens. In 25 544 l ♀ and also in 25 545 l ♀, the superior part of the neck is somewhat

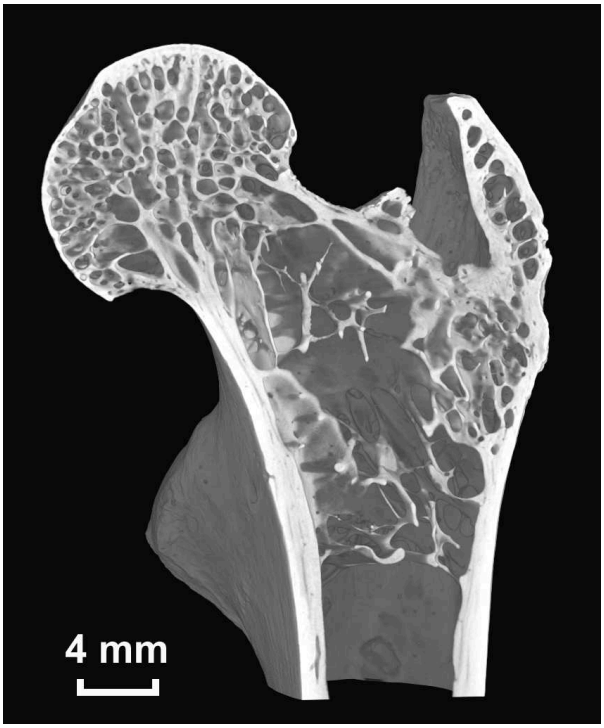

Figure 4.1: Ventral view in the trabecular architecture of the left femur of *Alouatta seniculus* 69.19 l ♂

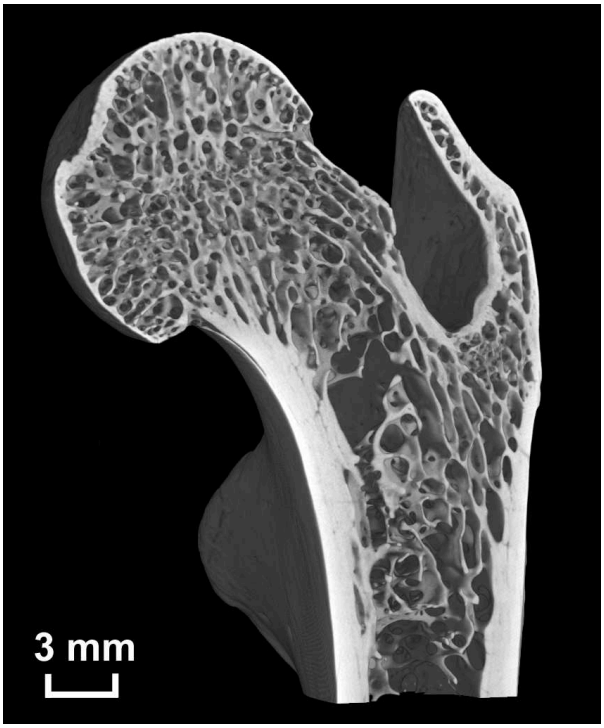

Figure 4.2: Ventral view in the trabecular architecture of the left femur of *Alouatta seniculus* 25 544 l ♀

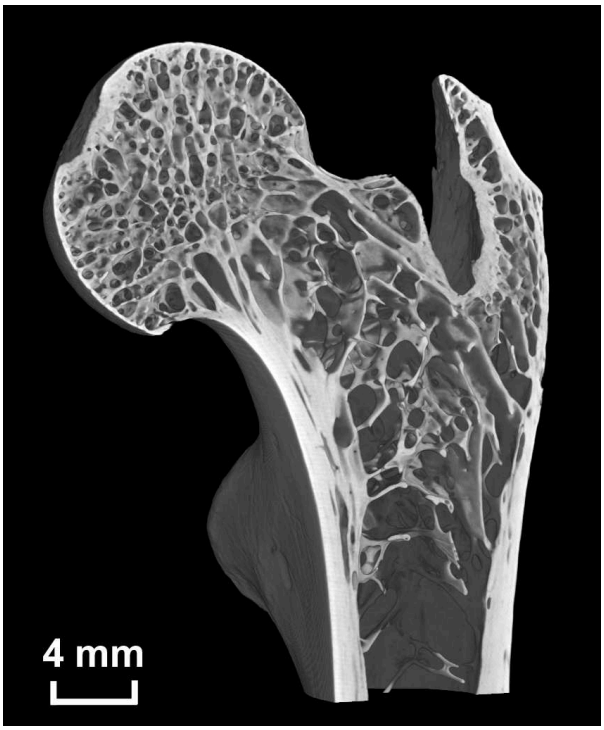

Figure 4.3: Ventral view in the trabecular architecture of the left femur of *Alouatta seniculus* 25 545 l ♀

filled by an extension of the second trajectorial sheaf coursing down form the femoral head. In all specimens, plate-like trabeculae create a substructure beneath the elongated bulge at the transition of the superior end of the femoral neck into the fossa trochanterica. These plates run parallel to the main positioning of the femoral neck and merge with each other posteriorly.

The greater trochanter is supported by a high density of trabecular plates (69.19 l ♂, 25 545 l ♀) or prolate trabeculae (25 544 l ♀). In its superior two-thirds these structures are inclined medially. At the transition of the greater trochanter to the main body of the femur a complex cancellous network is present. In this region plate-like trabeculae are dominant and are connected by rod-like trabeculae. Superiorly the trabeculae are aligned sub-parallel to the shaft axis and inferio-medially they align in the direction of the femoral neck.

The latter mentioned structures merge with the dispersed trabecular network coming down from the neck region. Large plate-like trabeculae and long rod-shaped trabeculae, both sparsely connected, dominate the region inferior to the greater trochanter. Superior-laterally in this region on 25 545 l ♀ and on 69.19 l ♂ and 25 544 l ♀ also in the center of this region the main direction of the cancellous bone follows the orientation of the femoral neck. Trabeculae in the medial and distal region are aligned perpendicular to the shaft axis. Lateral to the lesser trochanter, predominately plate-like trabeculae run sub-parallel to the shaft axis. Beneath the lesser trochanter itself a complex network of trabecular elements is present. Anteriorly on lesser trochanter, mainly plate-like trabeculae occur and lie in the median-sagittal plain (Figures 4.4

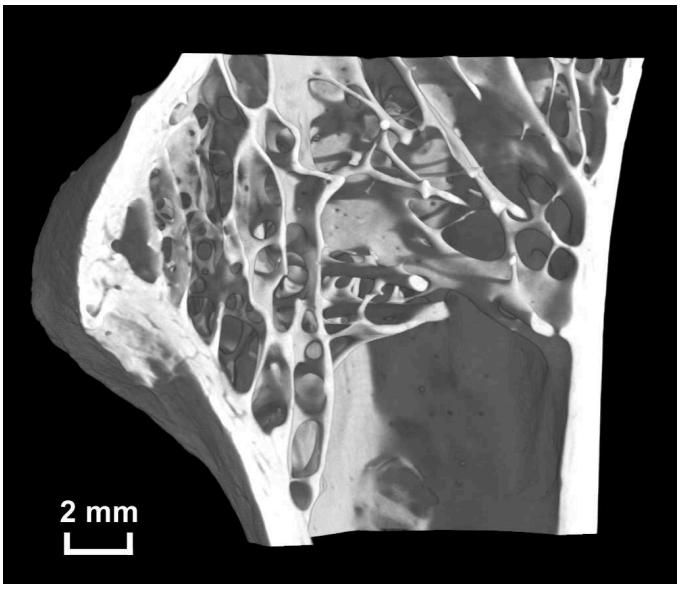

Figure 4.4: View in the trabecular architecture of the ventral third of the lesser trochanter of *Alouatta seniculus* 69.19 l ♂

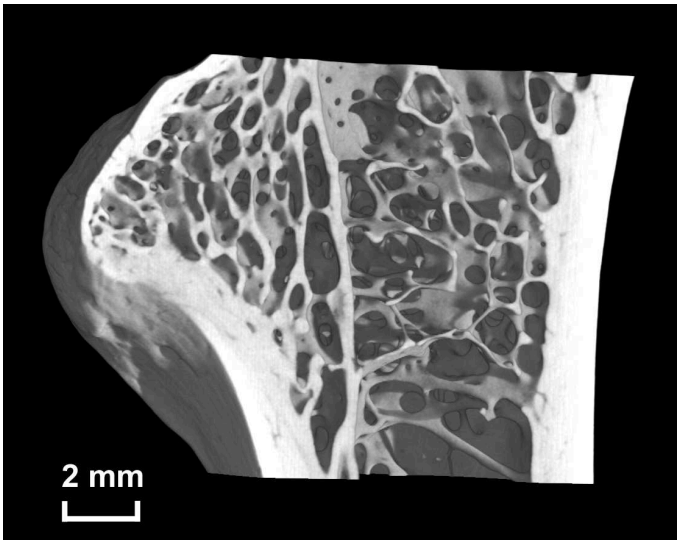

Figure 4.5: View in the trabecular architecture of the ventral third of the lesser trochanter of *Alouatta seniculus* 25 544 l ♀

and 4.6). This is seen most prominently in specimens 69.19 l ♂ and 25 545 l ♀. In 25 544 l ♀, these plate-like elements run in sagittally but they are slightly inclined towards the lateral (Figure 4.5). Posteriorly the trabeculae align in a sub-transverse plain. On 69.19 l ♂, prolate or rod-like trabeculae dominate posteriorly. In 25 545 l ♀ prolate and plate-like elements are common and in 25 544 l ♀ mainly plate-like trabeculae are seen posteriorly. However, due to increased trabecular density in nearly all regions, the trabecular architecture of 25 544 l ♀ contrasts with the other specimens although the general architectures are comparable.

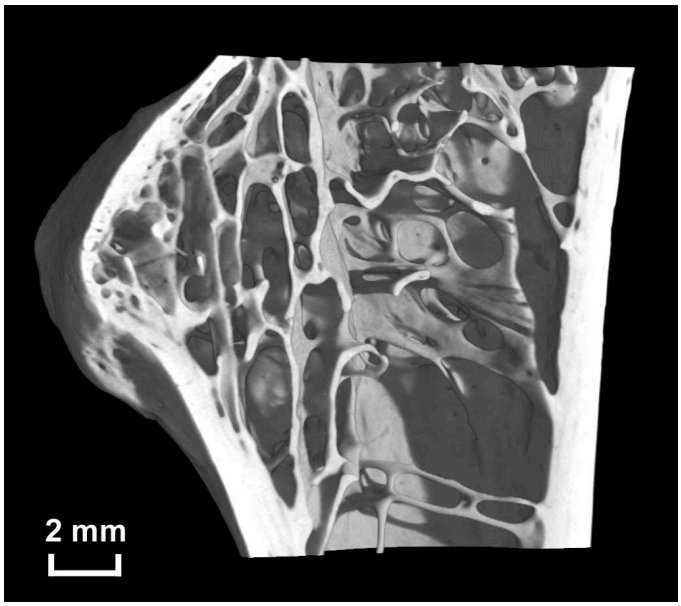

Figure 4.6: View in the trabecular architecture of the ventral third of the lesser trochanter of *Alouatta seniculus* 25 545 l ♀

Presbytis entellus

A high resolution CT image of *Presbytis entellus* 4743 l could not be obtained due to a metal nail in the femoral head was undetected during visual inspection and hindered the imaging procedure. Therefore, only the specimens 4734 l, 4745 l, and 4746 l are presented here. Compared to the *Alouatta seniculus* specimens, they have quite robust greater trochanters, femoral necks and heads. In their trabecular architecture, clear differences are visible when compared to the howler monkeys. Although both sample groups are quite similar in their outer femoral dimensions, the *Presbytis entellus* specimens exhibit a much denser, highly connected trabecular network.

All three Hanuman langur specimens are from juvenile individuals and show unfused epiphyses. A trajectorial bundle running from the inferior of the femoral neck completely through the femoral head is visible in all specimens (Figures 4.7, 4.8, and 4.9). Due to its advanced ontogenetic stage and thus epiphyseal fusion, the trajectorial bundle is best visible on 4734 l (Figure 4.7), while it is developed only faintly in the most immature specimen 4745 l (Figure 4.8). In 4745 l, the trabecular density is also the least of all three specimens.

Plate-like trabeculae dominate in the trajectorial structure and lie sub-parallel to the sagittal plain. The trajectory emerges clearly anteriorly and posteriorly in the femoral head. The whole trajectory extends quite far transversely, especially in 4746 l and, therefore, only small regions are not occupied by it. These are the medio-distal region, the latero-proximal region below the epiphyseal line, and the posterior and anterior-most regions in the superior half of the femoral head. In these areas the trabeculae are arranged radially from the joint surface. In the first two areas, prolate trabeculae dominate while in the latter regions above the epiphyseal line plate-like

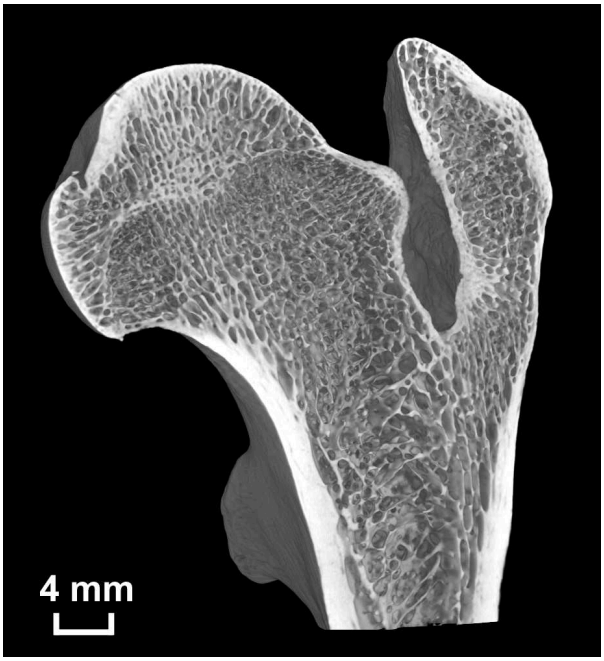

Figure 4.7: Ventral view in the trabecular architecture of the left femur of *Presbytis entellus* 4734 l

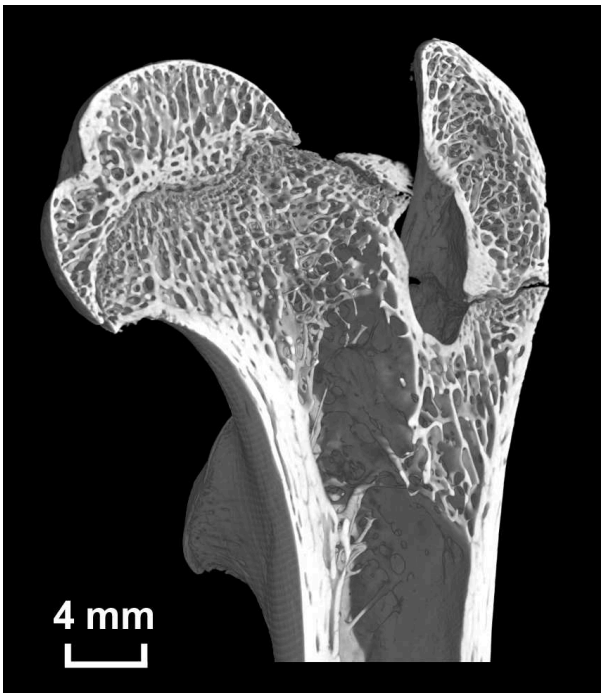

Figure 4.8: Ventral view in the trabecular architecture of the left femur of *Presbytis entellus* 4745 l

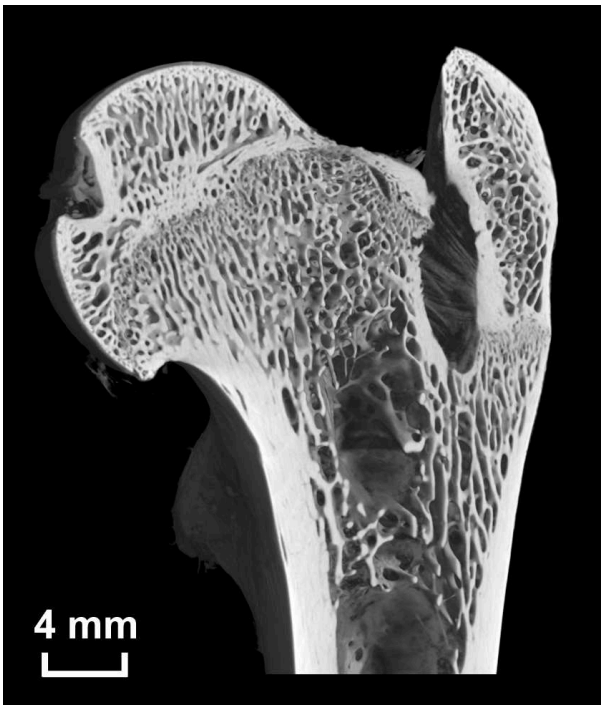

Figure 4.9: Ventral view in the trabecular architecture of the left femur of *Presbytis entellus* 4746 l

trabeculae are common. Above the epiphyseal line a generally condensed cancellous structure is present in the femoral head. As all specimens are immature, this feature could be linked with ontogenetic development.

The plate-like trabeculae of the trajectory of the femoral head extend into the neck and merge with the inferior cortex of neck or continue parallel to the cortex. In the posterior and medial-most regions plate-like elements dominate and extend in the same direction as the neck. Anteriorly at the disto-lateral end of the neck the trabeculae are running disto-medial to proximo-laterally, creating in this way another faint direction of alignment. These trabeculae are predominately of plate-like shape in 4746 l, while prolate trabeculae are common in 4734 l and rod-like structures dominate in 4745 l. In the ontogenetic more immature samples 4745 l and 4746 l the trabecular density decreases in the superior mid part of the neck and in the shaft region, causing a large open spaces.

In 4745 l and 4746 l, the epiphyseal split dissects the cancellous bone in the bulge between the superior end of the femoral and the fossa trochanterica, causing a less differentiated trabecular structure than in 4734 l. However, a consistent trabecular structure can be described in this bulge in all specimens. On the base of the bulge more (4746 l) or less (4734 l) plate-like trabeculae run parallel to the direction of the neck and in the superior part trabeculae align approximately perpendicular to the direction of neck and the cortical surface.

Concerning the greater trochanter no entire uniform architecture can be described for all three specimens. In 4746 l predominately plate-like trabeculae and some prolate elements are present. They are aligned laterally parallel to the cortical contour of the greater trochanter, while in the mid part and medially they orient perpendicular to the cortex. 4745 l shows in some parts a similar architecture except medially and in the mid part of the anterio-distal region of the greater trochanter where the trabeculae are aligned roughly longitudinally. In 4745 l the trabeculae are mainly of prolate shape, except in the lateral and proximo-anterior region where plate like elements dominate. In 4734 l a mixture of intensely connected small plate-like and prolate elements is present and the gross architecture, especially posteriorly is comparable to 4746 l. Anteriorly, a complex 3D network of mainly prolate and rod-like trabeculae take place and the two main directions of alignment described for 4746 l penetrate each other. The transition of the greater trochanter to the shaft is displayed clearest in 4734 l, as the epiphyseal split is already closed in this specimen. In 4734 l and 4746 l all trabeculae in this region are aligned sub-parallel to the shaft axis. In 4745 l the trabeculae course sub-parallel to the direction of the neck. Plate-like elements dominate this region in 4746 l while 4734 l shows some prolate forms in addition and in 4745 l increases the amount of prolate trabeculae towards the anterior-most region.

In the juvenile samples 4745 l and 4746 l the lower-most part of the imaged area is free of cancellous bone and separated from an open space in the distal part of the neck by thick and sparsely connected trabeculae lying in a sub-transverse plain. These trabeculae are in 4745 l (Figure 4.8) mainly of rod-like shape, while in 4746 l (Figure 4.9) also plate-like elements occur. These trabeculae build in 4746 l at the level of the lesser trochanter a connection between plate-like, longitudinally directed trabeculae running down at the lateral side and plate-like trabeculae aligned sub-parallel to the neck at the medial side. In 4734 l a similar arrangement consists of a higher amount of trabecular elements and of prolate trabeculae which run sub-parallel to the endosteal surface. Large open spaces are not present in this specimen, but smaller free spaces can be seen at the level of the mid part of the lesser trochanter and inferiorly.

The lesser trochanter is in the juvenile specimens 4745 l and 4746 l laterally dissected by the epiphyseal split. Therefore, the trabecular architecture is quite less differentiated. In 4746 l (Figure 4.12) some plate-like trabeculae, extending sup-parallel in a sub-sagittal plain can be noticed. In 4745 l (Figure 4.11) a similar arrangement seems to be present but can not be described in detail due to the epiphyseal split. 4734 l (Figure 4.10) shows a clearer architecture. At its lateral transition towards the shaft plate-like elements align sub-parallel to a sub-sagittal plain while medially plate-like trabeculae incline towards the lateral side. The medial-most trabeculae cover an angle of approximately 45° with the sagittal aligned trabeculae at the lateral transition. The trabecular architecture of the lesser trochanter is made up of a mixture of prolate and rod-like trabeculae. Posteriorly mainly plate-like forms occur, while anteriorly prolate and rod-like shapes predominate.

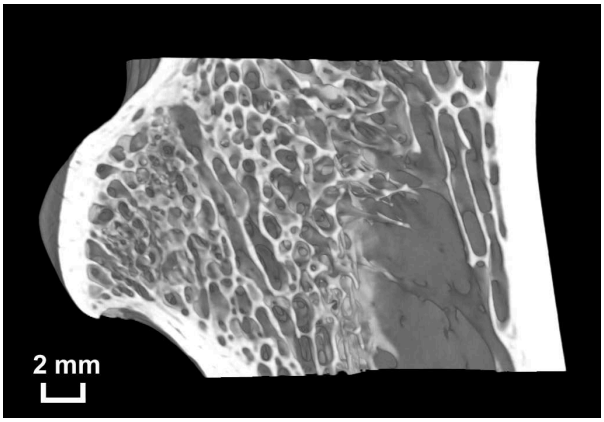

Figure 4.10: View in the trabecular architecture of the lesser trochanter of *Presbytis entellus* 4734 l

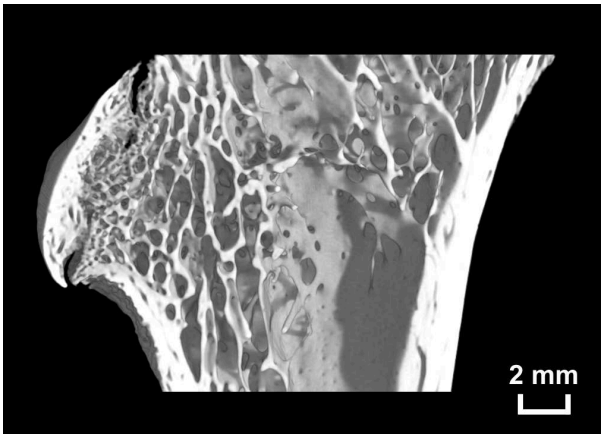

Figure 4.11: View in the trabecular architecture of the lesser trochanter of *Presbytis entellus* 4745 l

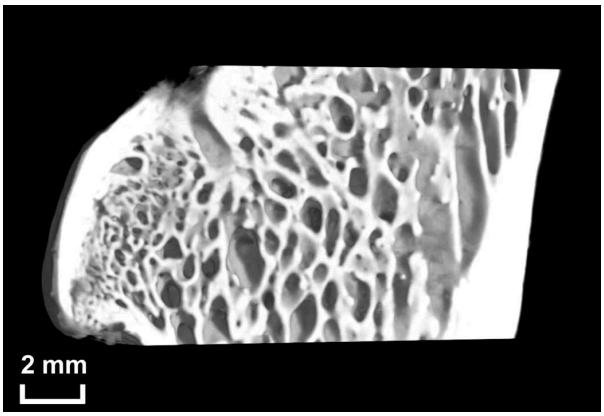

Figure 4.12: View in the trabecular architecture of the lesser trochanter of *Presbytis entellus* 4746 l

Papio hamadryas

Papio hamadryas displays a dense and highly connected cancellous bone structure with uniform features in the different parts of the femur (Figures 4.13, 4.14, 4.15, and 4.16). In the superior part of the femoral head a close network of relatively thick trabeculae is present. This feature is pronounced in the male individuals (Ha VIII 83 l ♂, Ha VIII 3 l ♂, 3212 l ♂) and consists mainly of plate-like trabeculae. In the female specimen (1.553 l ♀) only a faint increase in the thickness of the trabeculae, which are predominately of prolate shape, can be seen, while an increase in connectivity can not be noted. The sub-adult *Presbytis entellus* specimens show a similar feature above the epiphyseal split in the femoral head, therefore, it could be proposed that the *Papio hamadryas* specimens were also sub-adult. However, no epiphyseal split was found by close visual inspection of the *Papio hamadryas* specimens. The body weight, which is known for Ha VIII.83 l ♂ (24 kg) and Ha VIII 3 l ♂ (19.6 kg), exceeds the average weight of adult *Papio hamadryas* individuals, as noted by VAN HOOFF (1988), indicating that the specimens were probably full grown and that the above mentioned feature is not linked to an ontogenetic stage of development concerning *Papio hamadryas*. As this feature occurs very clearly in the male individuals which have a higher body weight (Table 2.5) and are bigger compared to the female specimen (Table B.26), it could be caused by the consequently higher loads which were induced upon the femora of the males.

At the proximal end of the inferior cortex of the femoral neck another structure emerges which can be assigned as trajectory and is build of plate-like trabeculae, lying in a para-sagittal plain. The trajectory courses steeply upward in direction of the superior part of the femoral head and penetrates the previously mentioned feature. In the intersection of both structures, each structure becomes increased. The trajectory extends less in transverse direction compared to a similar trajectory in *Presbytis entellus*. In the remaining parts of the femoral head radially arranged trabeculae can be discerned. These trabeculae have in 1.553 l ♀ predominately rod-like and prolate forms, while 3212 l ♂ and Ha VIII 3 l ♂ show mainly prolate and plate-like elements and in Ha VIII 83 l ♂ plate-like trabeculae with some few prolate elements dominate.

The trajectory extends along one third of the inferior cortex of the femoral neck. Towards the posterior side of the neck additional plate-like trabeculae occur, running parallel to the cortex while the connections between the trabeculae decrease and their thickness increases. The elevation separating the fossa trochanterica from the neck is pronounced in *Papio hamadryas*, especially in Ha VIII 83 l ♂, compared to the other species. Two structures meet in this elevation which are faintly developed and, therefore, can not be assigned as trajectories. The first one is just discernable anteriorly and runs diagonally from the lower cortex of the neck to the medial end of the fossa trochanterica at the superior cortex. In the anterior-most part this structure penetrates the second structure, while in the rear anterior half the first structure end at the second structure. Proximally the second structure dominates and follows the course of the cortex of the neck. Posteriorly the second structure also take place in those regions which were anteriorly occupied by the first structure and the intensity of the connections between

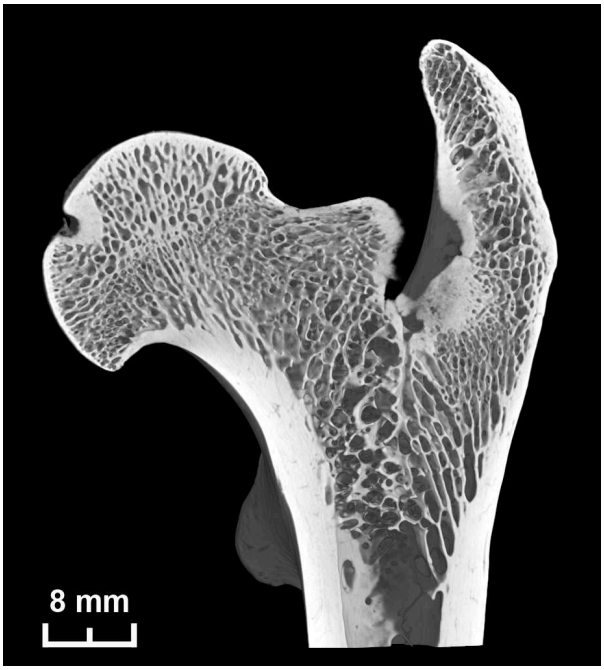

Figure 4.13: Ventral view in the trabecular architecture of the left femur of *Papio hamadryas* Ha VIII 83 l ♂

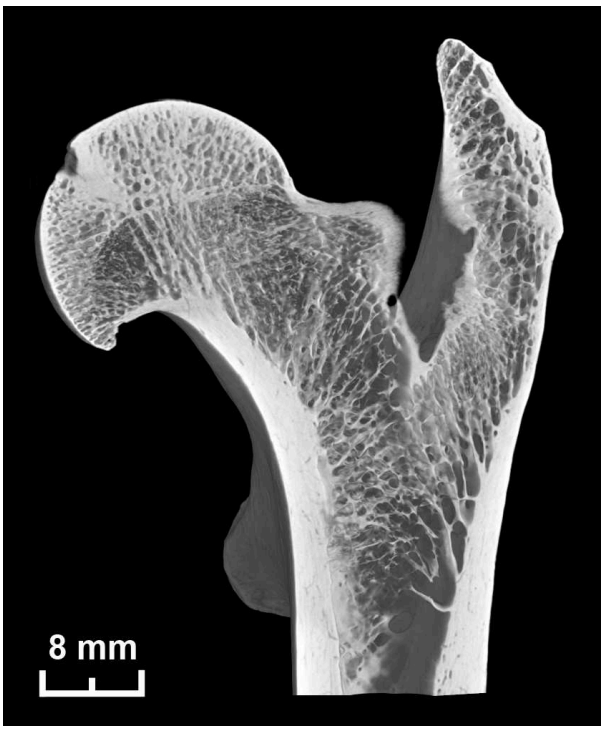

Figure 4.14: Ventral view in the trabecular architecture of the left femur of *Papio hamadryas* Ha VIII 3 l ♂

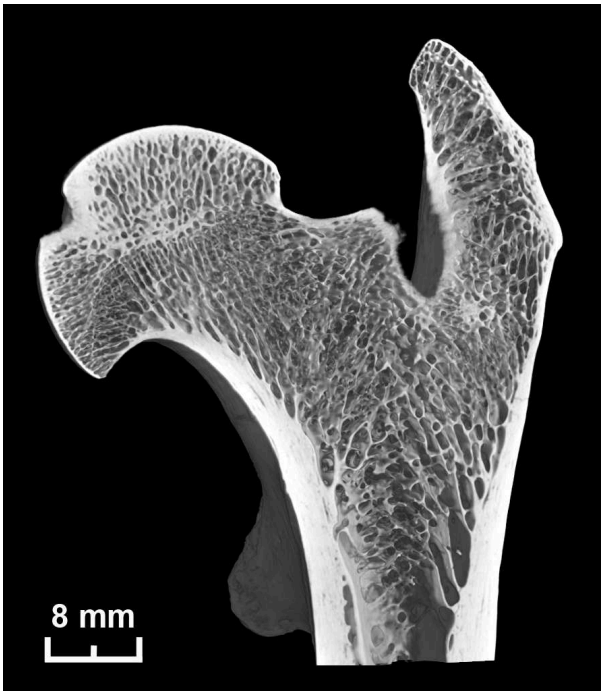

Figure 4.15: Ventral view in the trabecular architecture of the left femur of *Papio hamadryas* 3212 l ♂

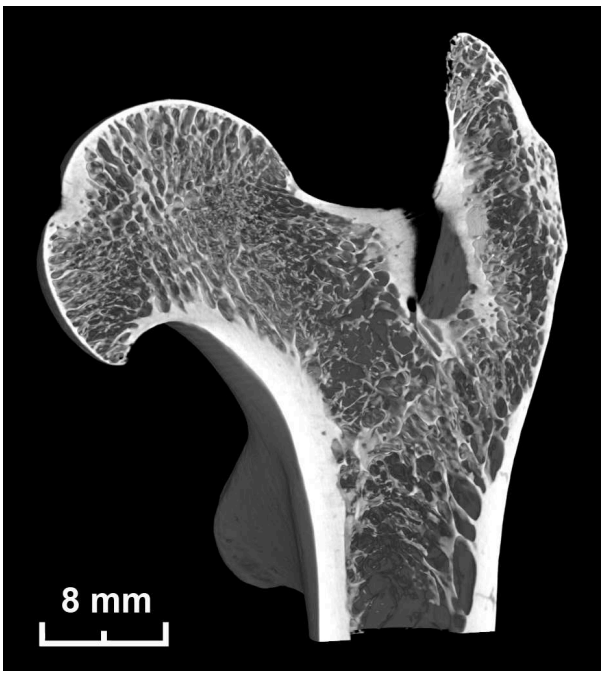

Figure 4.16: Ventral view in the trabecular architecture of the left femur of *Papio hamadryas* 1.553 l ♀

the trabeculae decreases while their thickness increases. In the proximo-posterior region of the elevation in Ha VIII 3 l ♂ and Ha VIII 83 l ♂ some trabeculae are aligned perpendicular to the cortex.

The first structure described above is build in Ha VIII 83 l ♂ of predominately plate-like and prolate forms and the second structure consists in the anterior-most region of prolate trabeculae while towards the posterior plate-like trabeculae increase. In Ha VIII 3 l ♂ prolate and rod-like elements dominate the first structure, which ends in this specimen at the cortex laterally beside the described elevation and do not course into the elevation. The second structure is build similar as in Ha VIII 83 l ♂, with a slightly higher amount of prolate forms. 3212 l ♂ shows in both structures mainly prolate trabeculae while anteriorly plate-like elements increase in the first structure.

The femur of the female individual 1.553 l ♀ is generally build of fine, rod-like and few plate-like trabeculae, forming a less dense network compared to the males. The elevation at the transition of the neck to the fossa trochanterica is of weak prominence on 1.553 l ♀, consisting mainly of cortical bone without a differentiated trabecular network supporting it. The two structures described above are just faintly visible, especially the second structure. Anteriorly between the two described structures and the trajectory extending from the femoral head into the neck, a triangle with a transition structure of mainly prolate trabeculae is present in all specimens.

The trabecular architecture of the greater trochanter shows uniform characteristics which are present in all specimens and exhibit some similarities to *Presbytis entellus*. The characteristics of Ha VIII 83 l ♂ are described first, as this specimen, the biggest of this sample, shows all features very well. Posteriorly the superior two-thirds of the greater trochanter consist of plate-like and prolate trabeculae which are inclined medially. The angle of incidence increases in proximal direction. These trabeculae are connected by predominately prolate elements under about right angles. Anteriorly the connections between the trabeculae decrease while their thickness increase. Laterally thick, plate-like trabeculae extend parallel to the contour of the lateral cortex and increase in number in anterior direction. In the transition area towards the shaft an area of undirected trabeculae can be discerned. Latero-distally plate-like trabeculae extend parallel to the lateral cortex. Medially to these trabeculae prolate and plate-like trabeculae incline laterally merging with the sheaf of plate-like trabeculae running down obliquely from the lateral end of the superior cortex of the neck in direction to the lateral cortex. This sheaf has about the same course as the neck and consists of relatively thick, plate-like and sparsely connected trabeculae. In Ha VIII 3 l ♂ and 3212 l ♂ a similar architecture but with less plate-like elements is present. 1.553 l ♀ has even fewer plate-like trabeculae and is generally composed of finer elements compared to the former two specimens .

In Ha VIII 83 l ♂ the trabeculae fade distally of the level of the lesser trochanter. At the lateral side of this region the sheaf of plate-like trabeculae originating at the lateral end of the superior cortex of the neck, extends distally. At the beginning of the posterior half of the

femur plate-like trabeculae run medially parallel to the medial cortex and increase in number posteriorly. Between these two structures and connected to the anterior cortex plate-like and rod-like trabeculae extend in a sub-transverse plain. The trabecular arrangement is quite similar in all specimens. The plate-like structure at the medial side is in Ha VIII 3 l ♂ restricted to the posterior-most part and the sub-transverse trabeculae in the mid part have predominately prolate and rod-like shapes. In 3212 l ♂ the medial structure is also anteriorly present and the sub-transverse trabeculae have mainly rod-like shapes. In 1.553 l ♀ the cancellous bone extends nearly until the distal end of the imaged area, even though few trabeculae are present at the medial side. The sub-transverse structure in the mid part consists in 1.553 l ♀ of mainly prolate and plate-like elements.

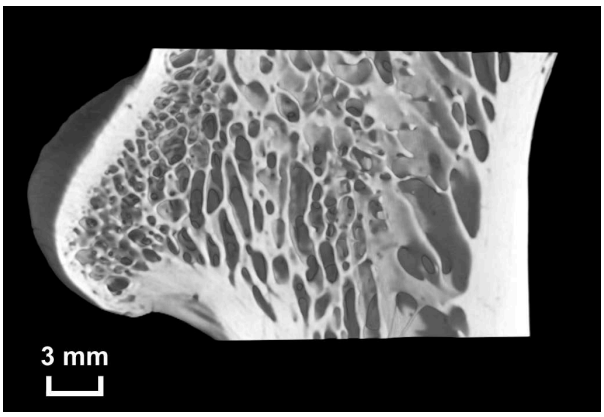

Figure 4.17: View in the trabecular architecture of the anterior half of the lesser trochanter of *Papio hamadryas* Ha VIII 83 l ♂

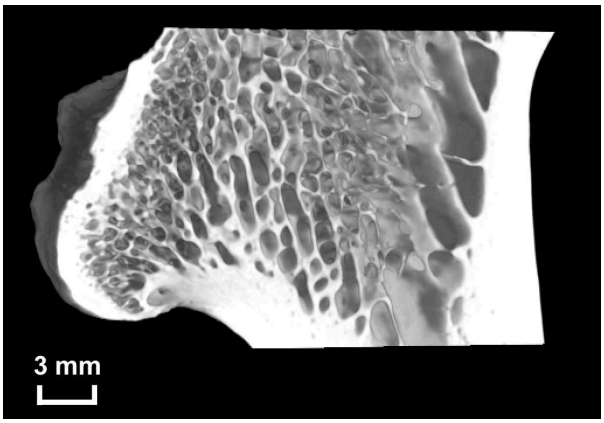

Figure 4.18: View in the trabecular architecture of the anterior half of the lesser trochanter of *Papio hamadryas* 3212 l ♂

The trabecular network of the lesser trochanter is quite uniform in all specimens, only the shape of the trabeculae differs between the specimens. Anteriorly the trabeculae lie around a sub-sagittal plain and are inclined laterally. Towards the posterior a fine network without a definite alignment is present first, while further posterior the trabeculae are aligned in a sub-

transverse plain. The anterior half in Ha VIII 83 l ♂ (Figure 4.17) is build by mainly plate-like elements, posteriorly prolate and plate-like trabeculae dominate. 3212 l ♂ (Figure 4.18) shows a similar architecture, but with a higher amount of plate-like trabeculae posteriorly. The laterally inclined structure in the anterior half is in Ha VIII 3 l ♂ just faintly discernible (Figure 4.19) and the amount of plate-like forms is definitely lower than in Ha VIII 83 l ♂. The posterior structure is in both specimens comparable. 1.553 l ♀ (Figure 4.20) shows throughout its lesser trochanter predominately prolate and rod-like trabeculae.

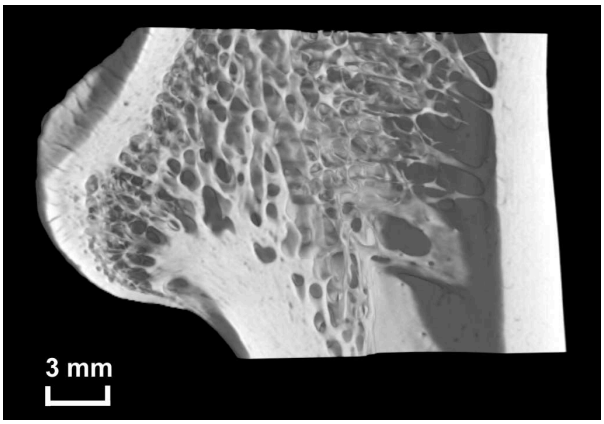

Figure 4.19: View in the trabecular architecture of the anterior half of the lesser trochanter of *Papio hamadryas* Ha VIII 3 l ♂

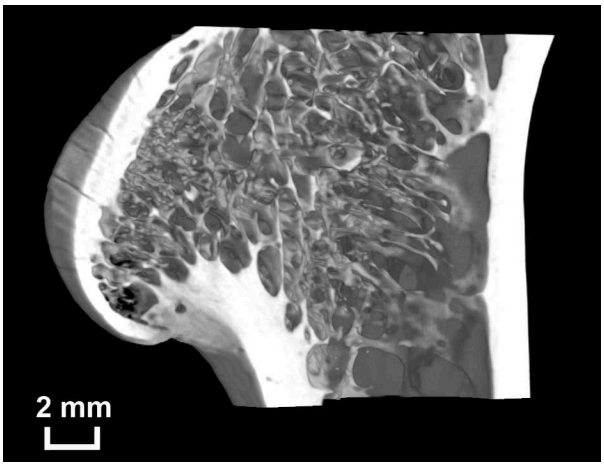

Figure 4.20: View in the trabecular architecture of the anterior half of the lesser trochanter of *Papio hamadryas* 1.553 l ♀

Hylobates seniculus / lar moloch

The trabecular architecture in *Hylobates lar moloch* 47 979 r ♂ (Figure 4.21) will be described first. It is at all more dispersed compared to *Alouatta seniculus*. The cancellous bone of the femoral head is build by widely separated and sparsely connected plate-like trabeculae. In the

center of the femoral head the cancellous network becomes condensed, as the intertrabecular distances become smaller, the connections between the single elements increase, and the spaces enclosed by the trabecular decrease. The trabeculae beneath the articular surface are all arranged radially and no real trajectorial structure can be detected.

However, plate-like trabeculae extend from the neck into the femoral head and can be tracked until the mid part of the femoral head. In the posterior part of the neck these trabeculae run parallel to the cortex of the neck and anteriorly they build two sheaves. Those trabeculae next to the superior cortex are aligned parallel to it, while those trabeculae adjoining the inferior cortex enclose an angle of approximately 30° with the cortex. The two trabecular sheaves are connected in the proximal mid part of the neck by plate-like elements. Distally the mid part begins to resolve and prolate and rod-like trabeculae with few connections and relatively large distances to each other occur. In the inferior most part these elements build connections between the anterior and posterior cortex of the neck.

The bulge at the transition of the neck to the fossa trochanterica is clearly developed. It is build by plate-like trabeculae which run approximately parallel to the neck and which are connected by prolate and rod-like elements.

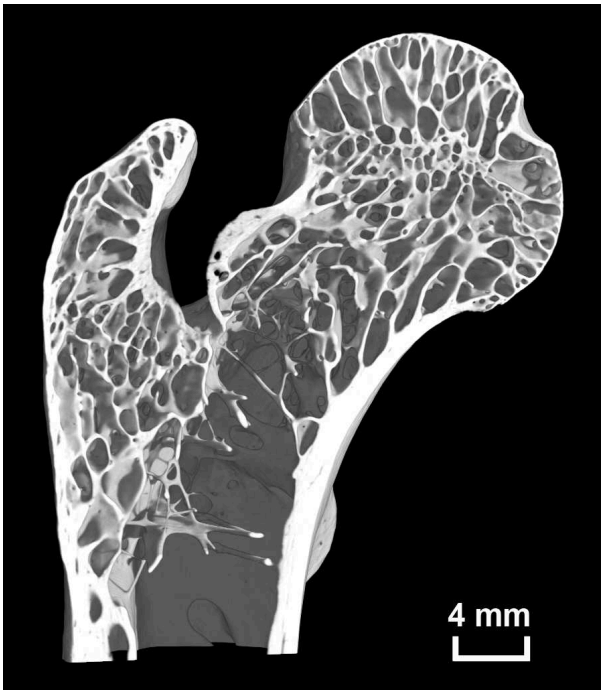

Figure 4.21: Ventral view in the trabecular architecture of the right femur of *Hylobates lar moloch* 47 979 r ♂

The cancellous bone of the greater trochanter is comparable to *Papio hamadryas* even so the greater trochanter is much smaller on *Hylobates lar moloch*. It is primarily made up plate-like trabeculae. In the superior most and anterior-most part the trabeculae are inclined medially and sparsely connected while in the inferior half they are reoriented and inclined towards the

lateral side. In the posterior-most part this structure gets replaced by an undirected cancellous bone structure. At the beginning of distal half plate-like trabeculae occur laterally and follow the contour of the cortex.

Distally to the greater trochanter plate-like trabeculae run parallel to the lateral cortex and continue until the end of the imaged area. In the adjoining mid part steeply inclined plate-like trabeculae come down from the superior cortex of the neck. Anteriorly these trabeculae are relatively thick with few connections to each other and relatively wide separated from each other. Posteriorly the thickness and the distances between the elements decrease while the connections slightly increase by prolate and rod-like trabeculae. Between this structure and the medial endosteal surface predominately thin, prolate and rod-like trabeculae extend. They lie around the transverse plain and are sparsely connected to each other and widely separated from each other. An exception is a big prolate trabecula above the beginning of the lesser trochanter, which directly connects the anterior and the posterior cortex. However, all these elements fade distally. Laterally to the lesser trochanter thick, plate-like trabeculae extend parallel to the medial endosteal surface. The cancellous bone network of the lesser trochanter is dominated by plate-like trabeculae (Figure 4.22). Laterally they are aligned sub-parallel to the shaft axis and in the anterior half the medial trabeculae incline laterally, while in the posterior half they pass into an undirected network.

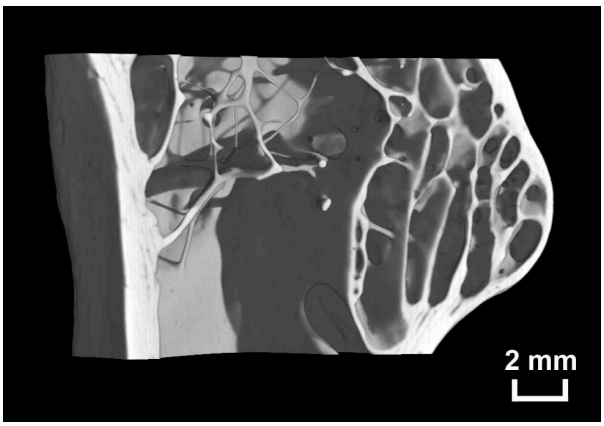

Figure 4.22: View in the trabecular architecture of the anterior half the lesser trochanter of *Hylobates lar moloch* 47 979 r ♂

Compared to *Hylobates lar moloch* 47 979 r ♂ the specimens of *Hylobates syndactylus* (6983 l ♂, 52.36. l ♀) (Figures 4.23, 4.24) have a similar cancellous bone architecture. The size difference between the two species could be responsible for the higher density of trabeculae in *Hylobates syndactylus*. The trabecular architecture of the femoral head of 6983 l ♂ and 52.36. l ♀ is comparable to 47 979 r ♂. The trabeculae below the articular surface are radially arranged and have mainly plate-like and prolate shapes in 52.36. l ♀, while in 6983 l ♂ the prolate forms predominate. Two trabecular sheaves of mainly plate-like trabeculae extend from the femoral neck into the head. However, a region with condensed trabecular bone in the middle of the

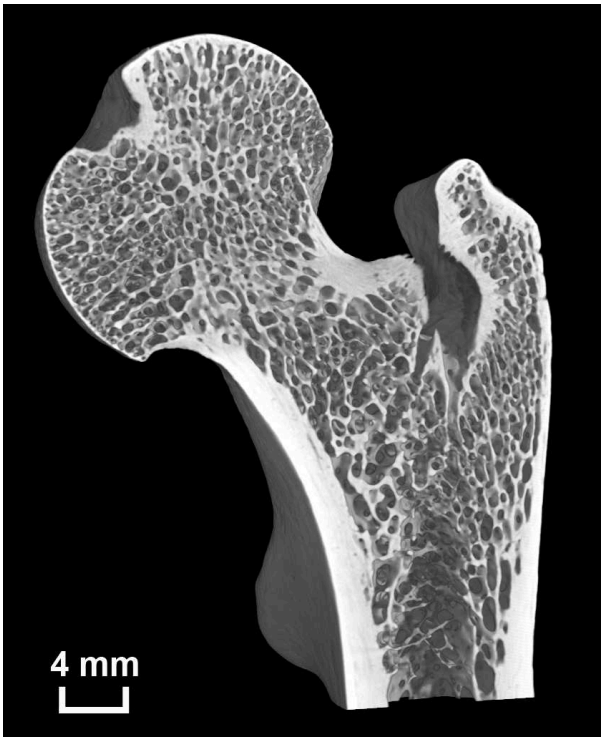

Figure 4.23: Ventral view in the trabecular architecture of the left femur of *Hylobates syndactylus* 6983 l ♂

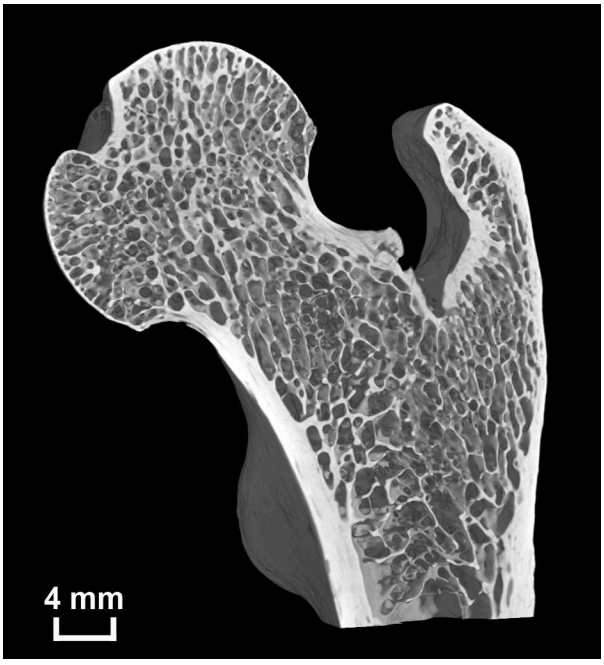

Figure 4.24: Ventral view in the trabecular architecture of the left femur of *Hylobates syndactylus* 52.36. l ♀

femoral head can not be detected in *Hylobates syndactylus*. Another difference compared to *Hylobates lar moloch* 47 979 r ♂ can be seen at a trabecular sheaf which crosses the femoral head in 6983 l ♂ and 52.36. l ♀ instead of fading in the mid part of the femoral head like in 47 979 r ♂. The sheaf originates at the inferior part of the neck, running upward obliquely and passes the femoral head ending at the cortex proximal to the fovea capitis. It builds a faint reinforcement structure which has no equivalent in *Hylobates lar moloch* 47 979 r ♂, although this structure is too feeble to be assigned as a real trajectory. It can be best seen in the posterior part of the femoral head of 6983 l ♂.

The gross architecture of the femoral neck in 6983 l ♂ and 52.36. l ♀ is comparable to 47 979 r ♂. Posteriorly mainly plate-like trabeculae align parallel to the main direction of the neck. Anteriorly the trabeculae split up in two trabecular sheaves. One sheaf is running parallel to the superior cortex of the neck, while the other sheaf extends next to the inferior cortex, enclosing an angle of around 30° with the cortex. Proximally the two sheaves are connected by prolate trabeculae (6983 l ♂) or prolate and rod-like trabeculae (52.36. l ♀). In the distal part of the neck the arrangement stays the same in 6983 l ♂, only the connections between the trabeculae decrease and the diameter of the trabeculae and the distances between them increase slightly. In 52.36. l ♀ the trabeculae fade posterio-distally and some small open spaces occur anteriorly in the mid part. The bulge on the neck superior to the beginning of the fossa trochanterica is mainly build of cortical bone. This bulge is on 52.36. l ♀ small and without any trabecular structure underneath it. In 6983 l ♂ some plate-like trabeculae occur, running parallel to the direction of the neck with few connections to each other, which are build by prolate or plate-like forms.

The trabecular architecture in the greater trochanter is in both specimens (6983 l ♂, 52.36. l ♀) comparable to 47 979 r ♂, except some differences anteriorly and posteriorly. In the anterior-most quarter of 6983 l ♂ the proximal-most trabeculae are inclined medially, while below this region an undirected network of cancellous bone takes place. A region of condensed bone is present in the mid part of the posterior half in 6983 l ♂. Distally to this structure all trabeculae are aligned almost parallel to the lateral cortex. 52.36. l ♀ shows just a thickening of the bone in the posterior-most mid part of the greater trochanter. However, in 6983 l ♂ generally prolate elements are present in the greater trochanter, while in 52.36. l ♀ predominately plate-like and prolate elements occur.

Distally to the main body of the greater trochanter similar structures as described in 47 979 r ♂ can be seen in 6983 l ♂ and 52.36. l ♀. The first structure consists of mainly plate-like trabeculae, which are aligned sub-parallel to the lateral cortex. They extend distally until the end of the imaged area. The second structure occurs laterally and consists of steeply inclined trabeculae, coming down from the superior cortex of the neck. 52.36. l ♀ shows this structure just posteriorly where it is build by plate-like trabeculae. This structure consists in 6983 l ♂ of a mix of prolate and plate-like elements and occurs throughout this part of the femur. Medially plate-like trabeculae run parallel to the medial endosteal surface. In contrast to 52.36. l ♀, 6983 l

♂ shows medially only few trabeculae. They are connected with the lateral structure by prolate (52.36. l ♀) or prolate and rod-like (6983 l ♂) trabeculae, which extend in a sub-transverse plain. These sub-transverse trabeculae also connect the anterior and posterior cortex and fade in distal direction, especially in 6983 l ♂.

The cancellous bone of the lesser trochanter is similarly arranged in 6983 l ♂ and 52.36. l ♀ (Figures 4.25, 4.26). It is bordered laterally by plate-like trabeculae, running almost parallel to the shaft axis. The remaining part consists anteriorly of trabeculae which are inclined laterally while posteriorly the trabeculae become aligned in sub-transverse direction.

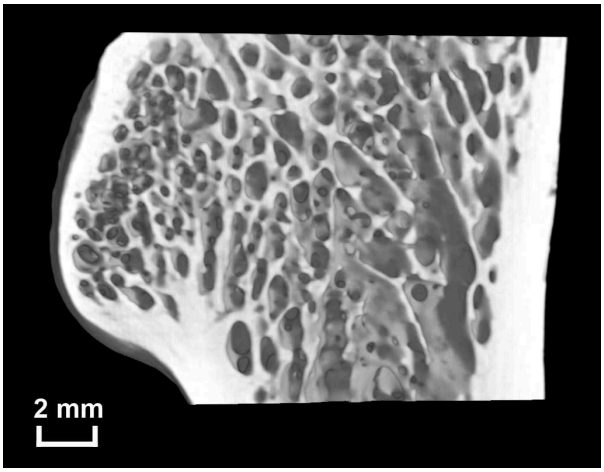

Figure 4.25: View in the trabecular architecture of the anterior half of the lesser trochanter of *Hylobates syndactylus* 6983 l ♂

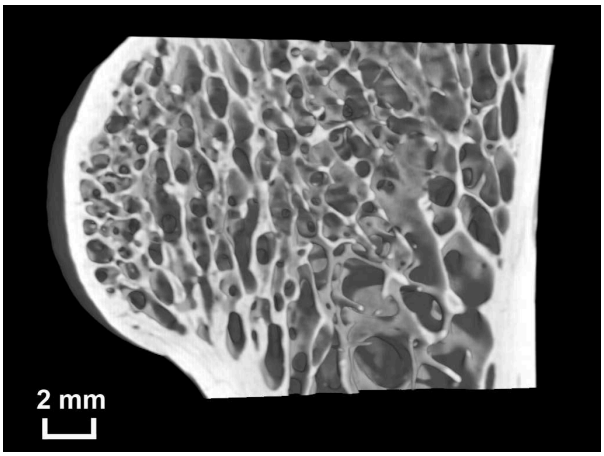

Figure 4.26: View in the trabecular architecture of the anterior half of the lesser trochanter of *Hylobates syndactylus* 52.36. l ♀

Homo sapiens

The cancellous bone structure of the human femur is well investigated. The known features could all be identified in the present sample and some further details could be described, too. Even so great importance was attached to image the specimens with the highest obtainable resolution and to display the trabecular architecture accurately, the shape of the single trabeculae could not be made visible as clearly as in the non-human specimens due to the fact that the focal distance of the high resolution CT system must be adjusted to the size of the specimen. Therefore, the maximal obtainable resolution refers to the size of the specimen and is in large objects always lower than in small objects.

All femora of *Homo sapiens* show similar characteristics in their cancellous bone architecture (Figures 4.27, 4.28, 4.29, and 4.30). Compared to the non-human specimens all human specimens lack the bulge at the transition of the neck to the fossa trochanterica. Another peculiarity in the human sample group is that all specimens display a thin bony layer which separates the proximal part of the femoral head from the distal part and in the mid third of the transition of greater trochanter to the shaft a condensed bone region can be noticed. These structures could both be a residuum of an epiphyseal split, even so almost all femora were from definitely adult individuals, except 22 l ♀(see Table 2.8).

The so called "compressive trajectory" is in all specimens clearly developed. It extends from the superior most part of the femoral head via the inferior part of the femoral neck to the medial side of the shaft, just above the level of the beginning of the lesser trochanter. As far as visible, due to the obtained resolution, the compressive trajectory consists of a high amount of prolate and some plate-like trabeculae. The second trajectory, known as "tensile trajectory", originates at the medial side of the femoral head and extends across the superior part of the neck to the lateral cortex of the shaft just below the greater trochanter. Compared to the compressive trajectory is the tensile trajectory somewhat fainter and in 10 l ♀ it is of weak prominence. In 21 l ♂ it is also quite weak, but stands out more clearly at the transition of the superior part of the neck to the femoral head and distally to the lesser trochanter. Except in 22 l ♀, where the tensile trajectory is quite strong developed, it is just discernible anteriorly. Another special characteristic in 22 l ♀ is that the tensile trajectory stand out clearly anteriorly against the cancellous bone of the greater trochanter. It seems that the amount of prolate and plate-like trabeculae is generally increased in the tensile trajectory compared to the compressive trajectory in all specimens.

Both trajectories are present in nearly all parts of the femoral head, just a small part in the medio-distal most region of the head is in 10 ♀, 11 l ♂, and 22 l ♀ not occupied by them and contains only few trabeculae. In 10 ♀ is the whole cancellous bone structure quite dispersed and just few trabeculae occur in the posterior-most part of the neck. The differences in the amount of trabeculae and the predominately rod-like shape of the trabeculae in 10 l ♀ might depend on age and size (see Table 2.8).

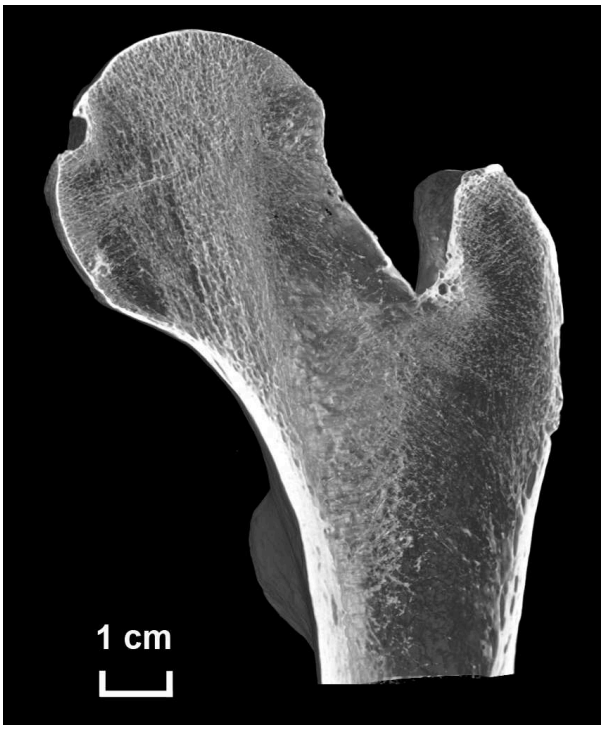

Figure 4.27: Ventral view in the trabecular architecture of the left femur of *Homo sapiens* 10 l ♀

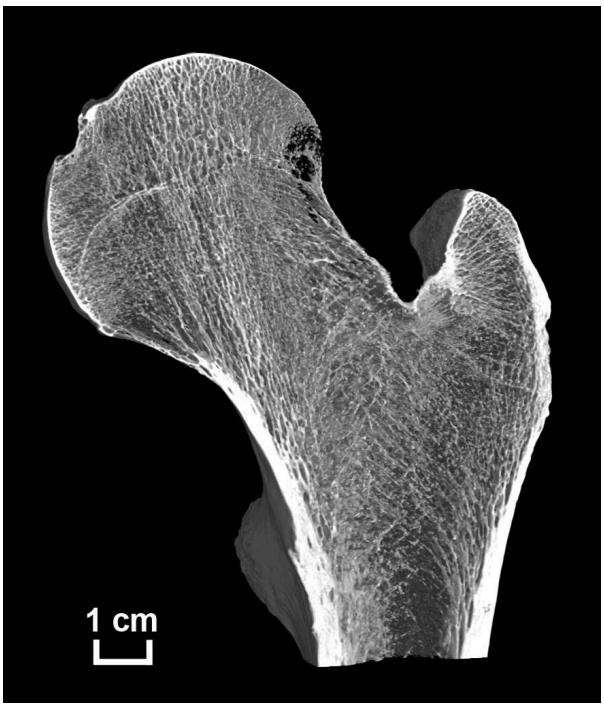

Figure 4.28: Ventral view in the trabecular architecture of the left femur of *Homo sapiens* 11 l ♂

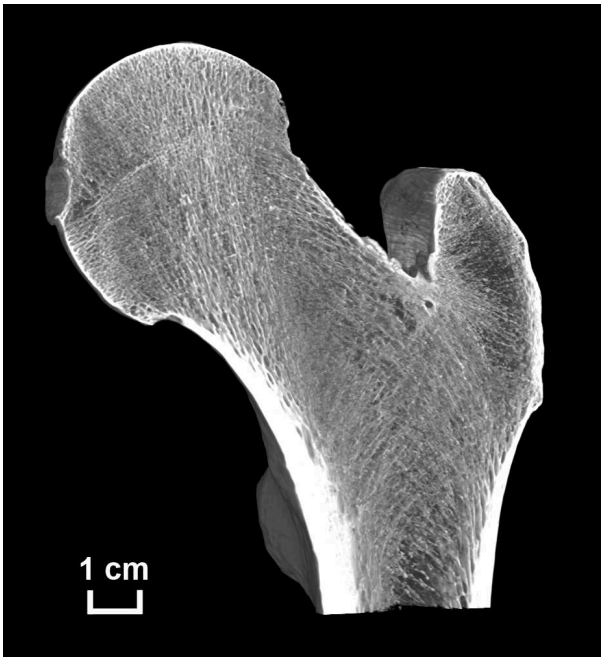

Figure 4.29: Ventral view in the trabecular architecture of the left femur of *Homo sapiens* 21 l ♂

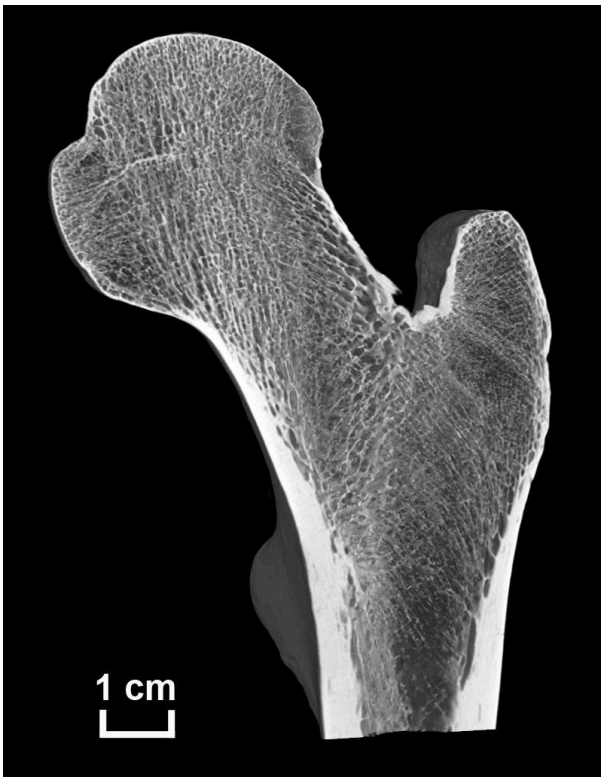

Figure 4.30: Ventral view in the trabecular architecture of the left femur of *Homo sapiens* 22 l ♀

The femoral neck is in its posterior-most part filled with trabeculae which run approximately parallel to the direction of the neck. The generally dispersed cancellous bone of the Ward's triangle is in all specimens made up of an undirected architecture. Another trajectory borders the Ward's triangle latero-distally. It extends diagonally from the medial cortex at the level of the proximal part of the lesser trochanter to the transition of the superior cortex of the neck into the fossa trochanterica. This trajectory, submitting predominantly tensile strains (VAN RIETBERGEN et al. 2003), is composed of trabeculae which are wider separated from each other and more sparsely connected with each other compared to the former mentioned trajectories. The shape of the single elements seems to be mainly prolate and rod-like. This trajectory stands out well in the two female specimens (10 l ♀, 22 l ♀) compared to the tensile trajectory in these specimens.

The greater trochanter is supported by a trabecular architecture comparable to the architectures described before in most of the non-human specimens, except *Alouatta seniculus*, although the whole structure consists of a higher amount of trabeculae in the human sample. Laterally plate-like trabeculae extend parallel to the lateral cortex. In the proximal part of the greater trochanter steeply medially inclined trabeculae are present. Towards the distal part these trabeculae reorient and incline laterally and merge further below with the tensile trajectory. In the region of the shaft at the level of the beginning of the lesser trochanter the tensile trajectory penetrates the trajectory which extends on the lateral side of the Ward's triangle. As a result of this penetration a pointed arch-like structure is present here. Distally to this region the cancellous bone begins to fade in distal direction in 10 l ♀, 11 l ♂, and 22 l ♀ while in 21 l ♂ the fading of the trabeculae begin further below, at the level of the distal part of the lesser trochanter. The cancellous bone of the lesser trochanter gets separated from the shaft region by prolate or plate-like trabeculae (Figures 4.31, 4.33, and 4.32). In 10 l ♀ these separating trabeculae are only discernible anteriorly (Figure 4.34). In the anterior half of the main body of the lesser trochanter the trabeculae incline slightly laterally, while towards the posterior half they begin to reorient, extending finally in a transverse plain. This reorientation begins in 10 l ♀ a bit further anterior and in 22 l ♀ not until the posterior third of the lesser trochanter.

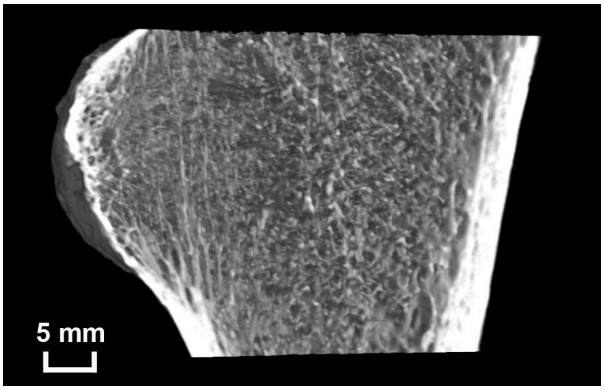

Figure 4.31: View in the trabecular architecture of the anterior half of the lesser trochanter of *Homo sapiens* 11 l ♂

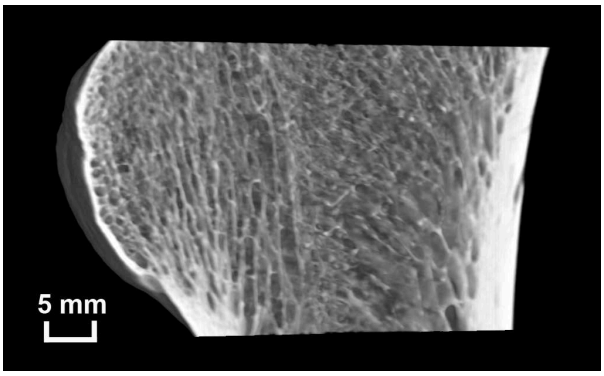

Figure 4.32: View in the trabecular architecture of the anterior half of the lesser trochanter of *Homo sapiens* 21 l ♂

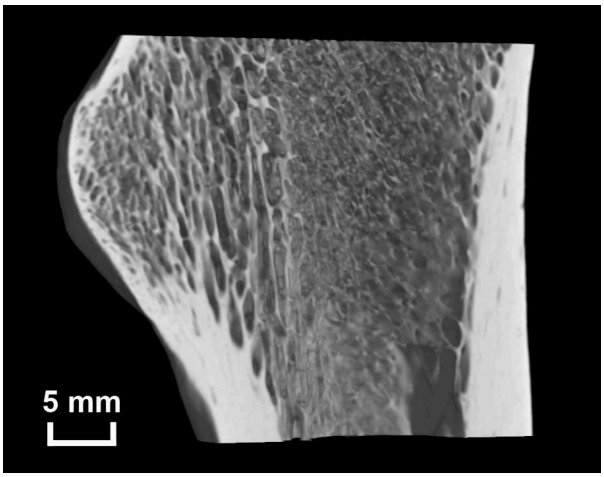

Figure 4.33: View in the trabecular architecture of the anterior half of the lesser trochanter of *Homo sapiens* 22 l ♀

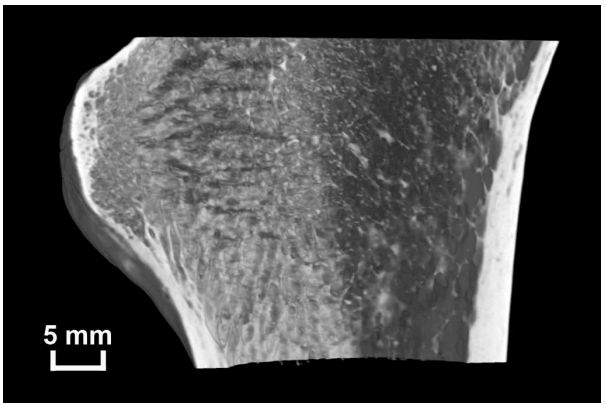

Figure 4.34: View in the trabecular architecture of the anterior half of the lesser trochanter of *Homo sapiens* 10 l ♀

Pliopithecus vindobonensis

It is note worthy that all *Pliopithecus vindobonensis* specimens posses a very uniform trabecular architecture (Figures 4.35, 4.36, 4.38, 4.39, and 4.40), even though it is difficult to see this architecture in 3D in specimen O.E. 560 l due to the filling (Figure 4.37). While unfused epiphysis are discernible on the outside of O.E. 560 l and 1970/1398/2 l, as mentioned in chapter 4.1.6, Zapfe (1960) noted that all *Pliopithecus vindobonensis* femora of the present sample show epiphyseal boundaries in radiographies. The high resolution CT images can not proof this statement, as no clear epiphyseal split is visible in all specimens.

The proximal third of the cancellous bone of the femoral head is build by relatively thick and wide separated plate-like trabeculae which are less connected to each other compared to the remaining trabeculae of the femoral head. These trabeculae are aligned perpendicular to the superior cortex of the femoral head. Distally to this structure a dense network of thinner trabeculae is present. A trajectory, extending from the proximal part of the inferior cortex of the neck to the superior end of the femoral head penetrates the structures described above. This trajectory is build of relatively thick and plate like trabeculae. It is visible throughout the femoral head, except in the anterior-most and posterior-most region. In the trajectory-free regions radially arranged trabeculae dominate.

Another quite directed structure, which may be classified as a trajectory, runs sub-parallel to the superior cortex of the femoral neck. It extends into the femoral head and ends in its the mid part at the dense network of thin trabeculae. This potential trajectorial structure is made up plate-like and prolate elements which are not as thick as in the previously described trajectory. The medial-most part of the femoral head, below the fovea capitis is occupied by plate-like and prolate trabeculae which are aligned approximately perpendicular to the medial cortex and also perpendicular to the strong trajectorial structure described above, which builds the lateral boundary of this region.

The anterior half of the femoral neck gets dominated by three structures. First plate-like trabeculae of the trajectory mentioned above which run sub-parallel to the inferior cortex of the neck. Distally the distances between these trabeculae increase and the thickness of the single elements slightly increase, while the connections between them decrease. The second structure is build by plate-like trabeculae running sub-parallel to the superior cortex, creating superiorly the potential trajectorial structure which continues into the femoral head. In the femoral neck these trabeculae are relatively thick, wide separated, and have few connections to each other while further anteriorly the intertrabecular distances decrease and the connections between the elements slightly increase. This second structure takes an arched course and extends distally to the lateral cortex at the level of the lesser trochanter. Only near the fossa trochanterica a slight interruption in its course is discernible. In the lateral extension of the second structure thick plate-like trabeculae dominate.

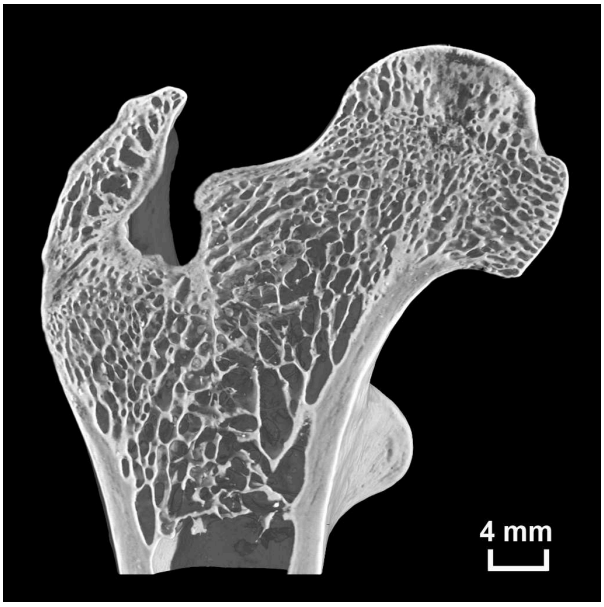

Figure 4.35: Ventral view in the trabecular architecture of the right femur of *Pliopithecus vindobonensis* O.E. 304 r

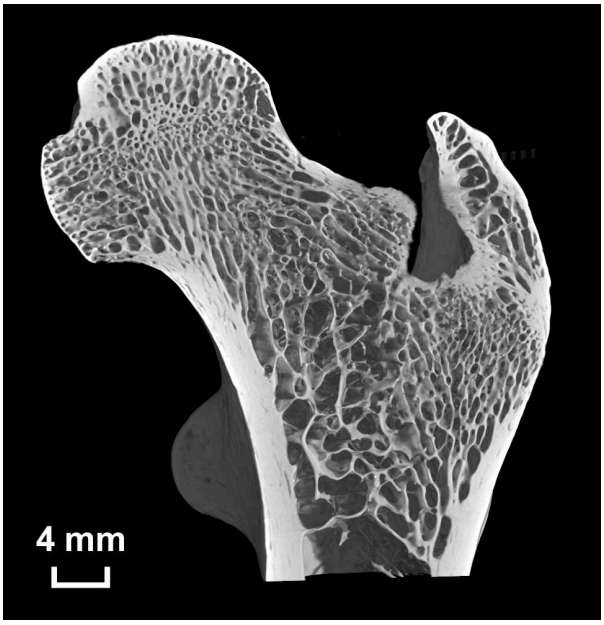

Figure 4.36: Ventral view in the trabecular architecture of the right femur of *Pliopithecus vindobonensis* O.E. 559 r

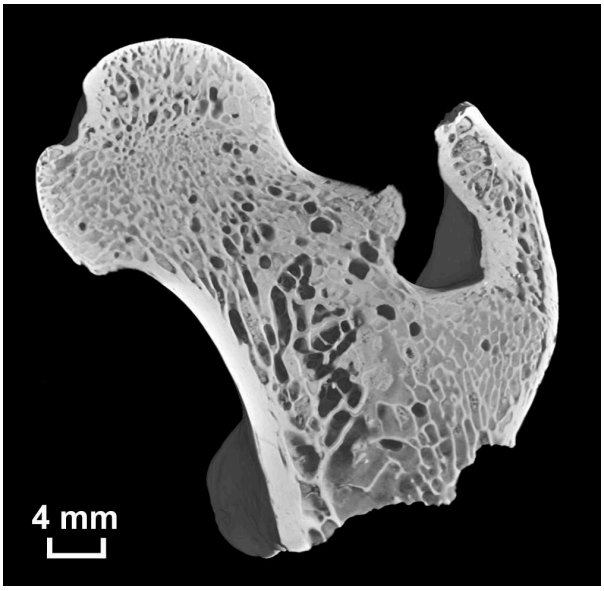

Figure 4.37: Ventral view in the trabecular architecture of the left femur of *Pliopithecus vindobonensis* O.E. 560 l

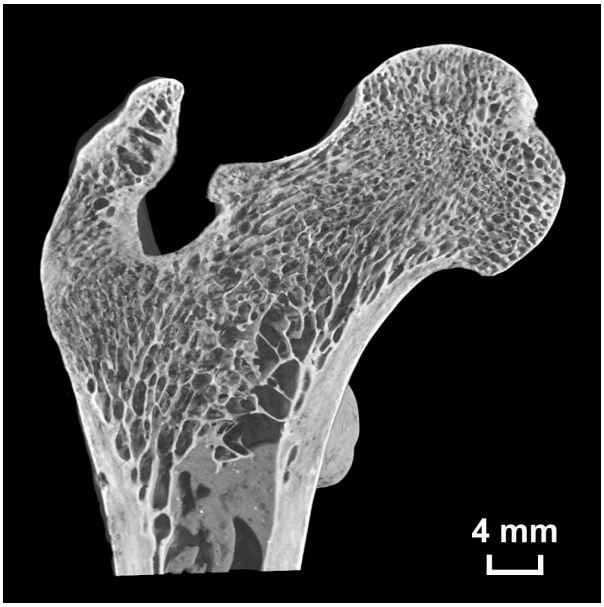

Figure 4.38: Ventral view in the trabecular architecture of the right femur of *Pliopithecus vindobonensis* 1970/1397/22 r

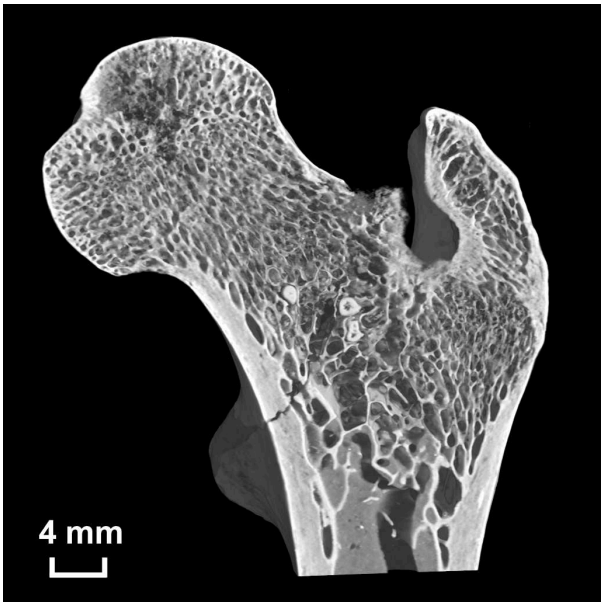

Figure 4.39: Ventral view in the trabecular architecture of the left femur of *Pliopithecus vindobonensis* 1970/1397/23 l

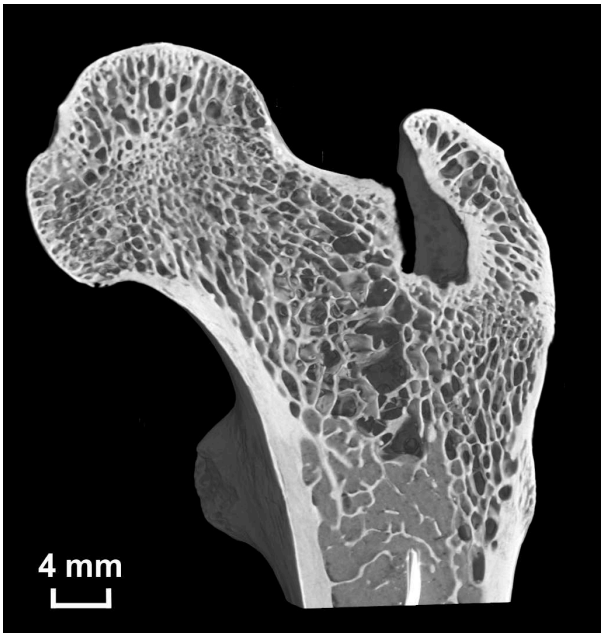

Figure 4.40: Ventral view in the trabecular architecture of the left femur of *Pliopithecus vindobonensis* 1970/1398/2 l

The second structure is very well developed in O.E. 559 l. Anteriorly between the previously described structures a third structure is present, consisting of a dispersed mixture of relatively thin plate-like, prolate, and rod-like trabeculae, without a definite direction of alignment. Posteriorly the first and the second structure merge, building a structure of plate-like trabeculae running parallel in the direction of the femoral neck.

An elevation between the fossa trochanterica and the superior cortex of the femoral neck is present on *Pliopithecus vindobonensis* like on the extant non-human specimens. This elevation contains mainly plate-like trabeculae aligned sub-parallel to the direction of the neck and connected to each other by prolate elements. The elevation is especially well developed in O.E. 304 r and O.E. 559 l where are also plate-like structures which are aligned approximately perpendicular to the cortical surface are present in its proximo-posterior region.

The main body of the greater trochanter contains laterally plate-like trabeculae which run parallel to the lateral cortex and increase in number towards the anterior. Prolate and plate-like trabeculae are aligned perpendicular to these trabeculae and incline by this way medially. The medially inclined trabeculae are relative thick, expect in the disto-anterior region. In the sagittal mid third of the greater trochanter, above the transition towards the distal part of the trochanter a region of condensed cancellous bone takes place. Distally to this region and anteriorly and posteriorly to the condensed cancellous bone, small plate-like trabeculae with prolate connections are present. These trabeculae run parallel to the lateral cortex, following its medially bent course and become stopped by the lateral part of the extension of the second structure of the neck described above.

The shaft region at the level of the lesser trochanter is often filled due to fossilization (O.E. 560 l, 1970/1397/22 r, 1970/1397/23 l, 1970/1398/2 l). As far as discernible at the filled specimens and by inferring from the not filled specimens (O.E. 304 r and O.E. 559 l), this region is occupied by a very dispersed network of plate-like and prolate trabeculae, extending around sub-transverse plains. These trabeculae are connected by rod-like and prolate elements.

The cancellous bone of the lesser trochanter is laterally bordered by plate-like trabeculae running sub-parallel to the shaft axis. The main body of the cancellous bone of the lesser trochanter can be separated in two halves. In the anterior half plate-like trabeculae inclining laterally dominate (Figures 4.41, 4.42, 4.43, 4.44, and 4.45) and in the posterior half a network of mainly prolate trabeculae extending around the transverse plain is present.

In O.E. 559 l and 1970/1398/2 l the directions of alignment are not as clearly developed as in the other specimens. Due to effects of fossilization the medial cancellous bone of the lesser trochanter is not well preserved in 1970/1397/23 l, obstructing a description of its trabecular architecture. The absence of parts of the lesser trochanter as well as the massive filling of the specimen made a description of the cancellous bone of the lesser trochanter in O.E. 560 l impossible (Figure 3.6).

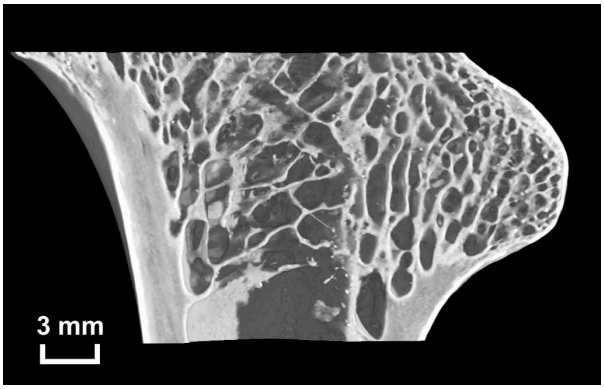

Figure 4.41: View in the trabecular architecture of the anterior half of the lesser trochanter of *Pliopithecus vindobonensis* O.E. 304 r

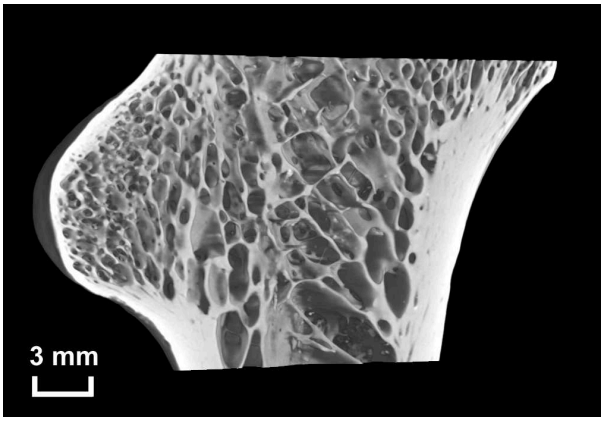

Figure 4.42: View in the trabecular architecture of the anterior half of the lesser trochanter of *Pliopithecus vindobonensis* O.E. 559 r

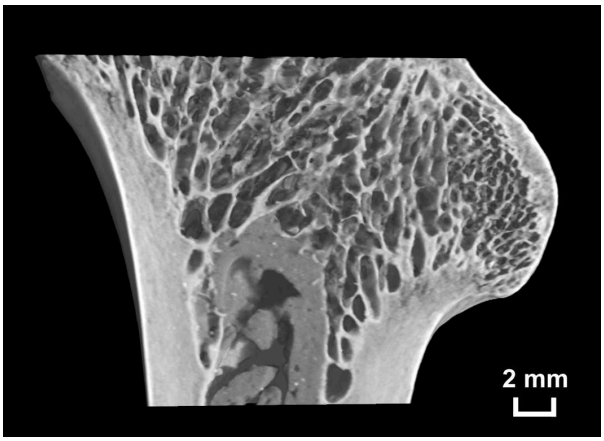

Figure 4.43: View in the trabecular architecture of the anterior half of the lesser trochanter of *Pliopithecus vindobonensis* 1970/1397/22 r

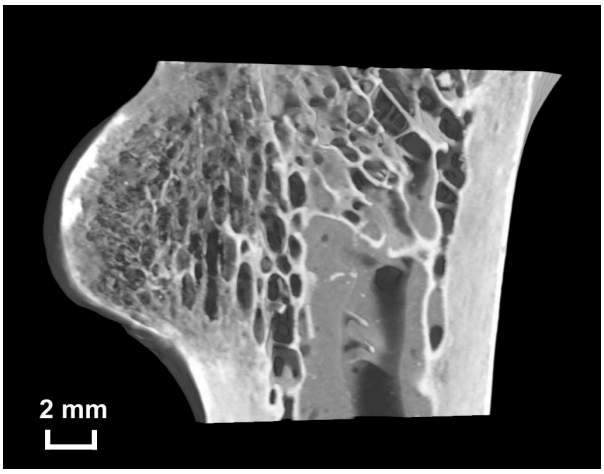

Figure 4.44: View in the trabecular architecture of the anterior half of the lesser trochanter of *Pliopithecus vindobonensis* 1970/1397/23 l

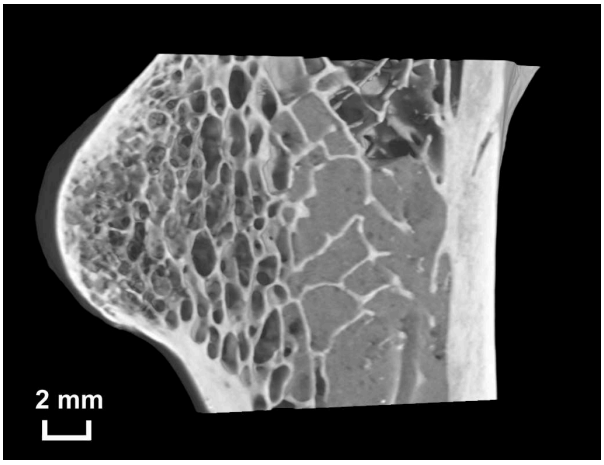

Figure 4.45: View in the trabecular architecture of the anterior half of the lesser trochanter of *Pliopithecus vindobonensis* 1970/1398/2 l

Paidopithex rhenanus

Paidopithex rhenanus is concerning its proximal femoral architecture quite similar to *Pliopithecus vindobonensis* (Figure 4.46). The proximal third of the femoral head consists of thick, wide separated plate-like trabeculae with relatively few connections to each other and a direction of alignment perpendicular to the articular surface. This region extends in *Paidopithex rhenanus* clearly medially beneath the fovea capitis unlike in *Pliopithecus vindobonensis*. A dense network of thin and mainly prolate shaped trabeculae lies next to this structure and occupies the mid region of the femoral head. In the medial part of the femoral head prolate and plate-like trabeculae, extending perpendicular to the medial cortex are present. These trabeculae end laterally at a trajectory which runs from the inferior cortex of the neck to the proximal end of the femoral head. The trajectory penetrates the structure mentioned first in the upper part of

the femoral head and in this way both structures become increased by each other. The distal extension of the trajectory runs sub-parallel to the inferior cortex of the neck, showing a coarser architecture build by thicker, more sparsely connected and wider separated trabecula, compared to the femoral head region.

Another structure runs around parallel to the upper cortex of the femoral neck. It extends proximally into the femoral head and distally towards the lateral cortex of the shaft. This structure is made of thick and wide separated trabeculae with few connections to each other. In the femoral head its architecture gets finer and it ends at the dense network of thin trabeculae in the middle of the femoral head. On its way to the lateral side of the shaft this structure gets slightly disturbed at the passage underneath the fossa trochanterica. In the proximo-anterior mid part of the femoral neck prolate and plate-like trabeculae are present, connecting the structure which runs parallel to the superior cortex of the neck and the extension of the trajectory, running sub-parallel to the inferior cortex of the neck. This connecting structure fades distally, giving way to open spaces. In the posterior part of the femoral neck the trajectory and the structure extending parallel to the superior cortex of the neck merge, creating a structure of plate-like trabeculae which extends parallel to the direction of the neck and runs into the femoral head. Distally this structure becomes more and more wide-meshed, but does not fade. In the bulge between fossa trochanterica and the superior cortex of the neck plate-like trabeculae run roughly parallel to the superior cortex. In the proximal most region of this bulge prolate trabeculae which are aligned perpendicular to the cortex are present.

As the proximo-posterior part of the greater trochanter is lacking, the description of its trabecular architecture can only refer to the remaining parts. In here many plate-like trabeculae,

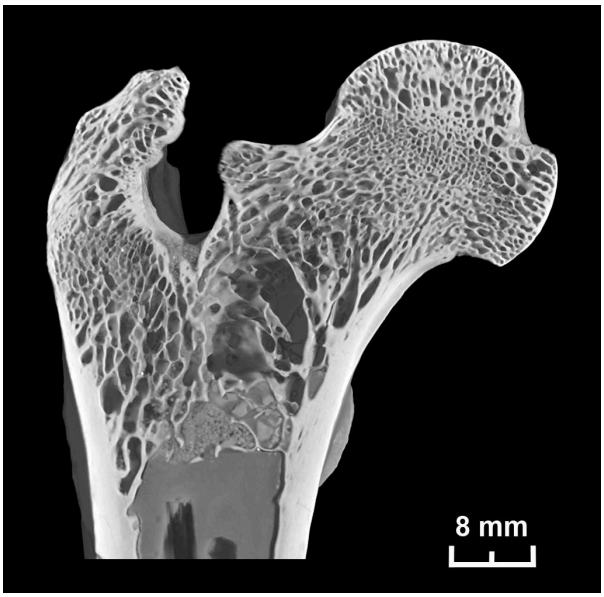

Figure 4.46: Ventral view in the trabecular architecture of the right femur of *Paidopithex rhenanus* Din 45 r

lying next to each other run sub-parallel to the lateral endosteal surface. At right angles to these trabeculae plate-like and prolate elements incline medially. Similar to *Pliopithecus vindobonensis* but less distinct and mainly at the lateral side, a condensed cancellous bone structure takes place in the mid part of the greater trochanter. Below this structure a fine-meshed network of relatively thin prolate and plate-like trabeculae is present. This network is aligned approximately parallel to the adjoining lateral cortex and gets in anterior direction step-by-step coarser, as the thickness of the trabeculae and the distances between them increase while the connections between them decrease. This network gets terminated by the extension of the structure which extends parallel to the superior cortex of the femoral neck.

A filling, partially anthropogenic due to glue, begins at the level of the lesser trochanter, permitting only a description of the trabecular architecture in the superior shaft region. In here plate-like trabeculae extend around the transverse plain and in oblique directions. The trabeculae lying sub-parallel to a transverse plain connect the plate-like trabeculae at the lateral cortex, coming down from the superior part of the neck, with plate-like trabeculae which run approximately parallel to the medial cortex. In the lesser trochanter plate-like longitudinally extended trabeculae with prolate connecting elements border its lateral side. The trabecular architecture of the lesser trochanter is anteriorly dominated by plate-like and prolate elements which incline laterally (Figure 4.47). The posterior half is partly damaged at the medial side, but nonetheless a reorientation of the trabeculae towards a sub-transverse plain can be noted.

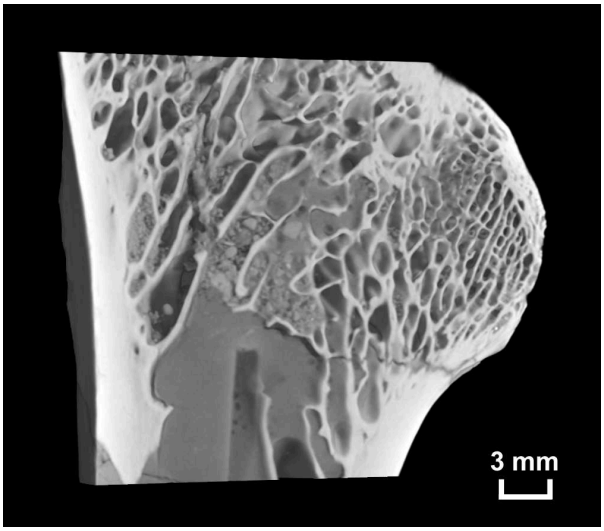

Figure 4.47: View in the trabecular architecture of the anterior half of the lesser trochanter of *Paidopithex rhenanus* Din 45 r

4.3.2 Histomorphometric results

When reviewing the different parameters obtained using the histomorphometric analysis (Table C.1 and C.2), a differentiation has to be made between parameters which depend on measures, such as the 'connectivity density' (Conn.Dens) [1/mm^3], the 'mean trabecular thickness' (Tb.Th) [mm], the 'mean trabecular separation' (Tb.Sp) [mm], and the 'mean trabecular number' (Tb.N) [1/mm], and non-dimensional parameters like the 'structure model index' (SMI) and the 'degree of anisotropy' (DA). The latter parameters describe architectonic characteristics which are hypothesized here to be independent of allometric effects. The load environments are presumed to cause definite loading directions making a certain alignment and definite shapes of the trabeculae necessary. However, the former parameters are also under the influence of the load magnitude and in this way affected by the size and weight of an individual. Body weight directly influences the stress intensity and strain rate of bone. Both of them have an effect on the bone mass (Lanyon 1981, Whalen et al. 1988, Rubin et al. 1990). Therefore, it was attempted to find a method to eliminate variation caused by weight and size and to extract only those differences which were caused by different types of habitual locomotion. The 'bone volume fraction' (BV/TV) is believed to be quite informative as this parameter includes an expression of a specimen size and weight. The bigger and heavier an individual is, the higher the BV/TV will be in theory as the BV increases by weight. The increase of TV with size is not estimated to be proportional with BV due to allometric effects. The assumption concerning the BV proved to be true regarding individual size in *Homo sapiens* and *Papio hamadryas*, which is in these two species related with sexual dimorphism, but not in *Alouatta seniculus* and *Hylobates seniculus* (Table C.1).

However, it must be mentioned that the sample size is too small to draw reliable conclusions about individual differences or sexual dimorphism but is big enough to make a qualitative discrimination of the different locomotor habits preferred by the different species. To reduce the size factor from the parameters mentioned above, they were set in proportion to the individual BV/TV. Table 4.2 and 4.3 show the size correction of these parameters. The adjusted parameters are marked by an asterisk in the following (Conn.Dens / (BV/TV) = *Conn.Dens**, Tb.Th / (BV/TV) = *Tb.Th**, Tb.Sp / (BV/TV) = *Tb.Sp**, Tb.N / (BV/TV) = *Tb.N**).

The *Conn.Dens** can be taken as a basic measure of the trabecular architecture as it describes the complexity of the network. The higher the *Conn.Dens** the more complex is the whole structure. By describing the structural measures of single components, like *Tb.Th**, *Tb.Sp** and *Tb.N**, the *Conn.Dens** yields a good discrimination of different trabecular architectures. The different species can be discriminated by diagrams in which the data for each species are pooled (Figures 4.48, 4.49, 4.50). An increase or decrease of trabecular bone volume as an effect of fossilization ion exchange (Ryan & Ketcham 2002a) cannot be excluded but the converse also not proved. Therefore, the obtained data, especially Tb.Th and *Tb.Th**, were presumed to be unaffected.

Pliopithecus vindobonensis has the highest *Conn.Dens** with an average *Tb.N** with relatively fine (*Tb.Th**) trabeculae which are close together (*Tb.Sp**). *Pliopithecus vindobonensis* slightly exceeds the values of *Presbytis entellus* by having more, thinner, less separated trabeculae, but both species always show share this trend. Except concerning the amount of trabeculae *Papio hamadryas* always lies in mid range and stays in a rather fixed relation to the *Presbytis entellus* data. *Alouatta seniculus* and the pooled *Hylobates seniculus / lar moloch* data show similar trends and lie in a similar distance to one another. *Alouatta seniculus* exceeds the *Hylobates* data in having relatively thick trabeculae which enclose the biggest space and the highest *Tb.N** of all species. *Paidopithex rhenanus* has a low *Conn.Dens** and the lowest *Tb.N** of all species and shows despite these differences an inverse relation to *Pliopithecus vindobonensis* and by this ways also to *Presbytis entellus* and *Papio hamadryas*. *Homo sapiens* has the lowest *Conn.Dens** and the thickest trabeculae (*Tb.Th**) even after size correction. The

Table 4.2: Size related parameters set in relation to BV/TV for extant species

	BV/TV [mm^3]	Conn.Dens/ (BV/TV) [$1/mm^3$]	Tb.Th/ (BV/TV) [mm]	Tb.Sp/ (BV/TV) [mm]	Tb.N/ (BV/TV) [1/mm]
Alouatta s. (69.19 l) ♂	0.1220	4.1598	2.0795	14.5525	4.4393
Alouatta s. (25 544 l) ♀	0.2843	10.2870	0.8020	3.0609	3.8983
Alouatta s. (25 545 l) ♀	0.1595	5.7473	1.4376	11.5480	3.5361
Presbytis e. (4734 l)	0.3840	3.3271	0.9109	2.8021	2.4974
Presbytis e. (4745 l)	0.2052	11.7890	1.1793	7.8533	3.2222
Presbytis e. (4746 l)	0.2969	11.0748	0.8050	3.1064	3.7127
Papio h. (1.553 l) ♀	0.2026	7.5903	1.2048	5.1964	4.7542
Papio h. (HA VIII 3 l) ♂	0.2438	3.6821	1.3491	4.6423	3.6768
Papio h. (HA VIII 83 l) ♂	0.2711	4.3729	1.1062	4.6079	3.0867
Papio h. (3212 l) ♂	0.2254	4.2822	1.3159	7.0470	3.0253
Hylobates l. m. (47 979 l) ♂	0.1272	3.3145	1.7162	18.1722	3.5582
Hylobates s. (6983 l) ♂	0.3419	6.7257	0.8833	3.0070	2.9936
Hylobates s. (52.36 l) ♀	0.2890	5.2097	1.0073	3.4654	3.3744
Homo s. (10 l) ♀	0.3007	2.5214	1.5750	3.7592	2.9268
Homo s. (11 l) ♂	0.4317	0.9801	1.6857	2.9907	1.7783
Homo s. (21 l) ♂	0.5934	0.3837	1.3851	1.6003	1.5359
Homo s. (22 l) ♀	0.3248	1.6598	1.8088	10.4637	1.1385

Table 4.3: Size related parameters set in relation to BV/TV for fossil species

	BV/TV [mm^3]	Conn.Dens/ (BV/TV) [1/mm^3]	Tb.Th/ (BV/TV) [mm]	Tb.Sp/ (BV/TV) [mm]	Tb.N/ (BV/TV) [1/mm]
Pliopithecus v. (O.E. 304 r)	0.2902	9.8356	0.7715	3.5134	3.6075
Pliopithecus v. (O.E. 559 l)	0.3225	7.6254	0.7786	3.3860	2.9950
Pliopithecus v. (1970/1397/22 r)	0.2951	15.2667	0.7245	3.3504	3.8285
Pliopithecus v. (1970/1397/23 l)	0.3184	12.4821	0.7591	3.1467	3.2073
Pliopithecus v. (1970/1398/2 l)	0.3133	8.7325	0.7491	2.8771	3.5110
Paidopithex r. (Din 45 r)	0.2770	2.4531	1.1733	8.5787	1.7119

*Tb.N** is relatively low and the spacing (*Tb.Sp**) is average. The data of *Homo sapiens* cannot be linked to other species.

The SMI data of the sample group gives a quantitative description of the trabecular forms prevailing in the ROI (Table C.1 and C.2). The SMI varies in the species, while in the whole sample it ranges mainly between 0.8914 (*Homo sapiens* 10 l ♀) and -1.2845 (*Paidopithex rhenanus* Din 45 r), with the exception of *Homo sapiens* 21 l ♂ (-3.7335). More than half the sample shows negative SMI values which track with high BV/TV values. This is in accordance with the analysis of SCANCO Medical AG who found that negative SMI occur between a BV/TV of 0.3 up to 0.4 (personal communication A. Laib, SCANCO Medical AG). The sample group shows some species specific variation but nonetheless follows the trend of negative SMI occuring in those specimen which show higher BV/TV values.

With regard to the analysis results comprising the whole ROI, the region around the lesser trochanter, which is composed of quite different architectonic areas, the particular SMIs are composite values of all trabecular forms of these areas. They can therefore not be directly linked to the descriptions of trabecular shapes made in chapter 4.3.1 but give an impression of the gross architecture.

The positive SMI values close to 0 indicate a structure of predominately plate-like trabeculae with some prolate and rod-like forms. The more negative the SMI, the more concave elements involved, for example openings in plate-like bone structure. A high negative SMI is an expression of an overall condensed, solid bone with some openings. However, in terms of the observed structures (see Chapter 4.3.1), the negative SMIs correspond quite well with an architecture made up of predominately large, plate-like elements with some small prolate or rod-like forms, connecting the plates between. Generally, good concordance between the SMI, defined as a gross architectonic measure and the observed architectures exist.

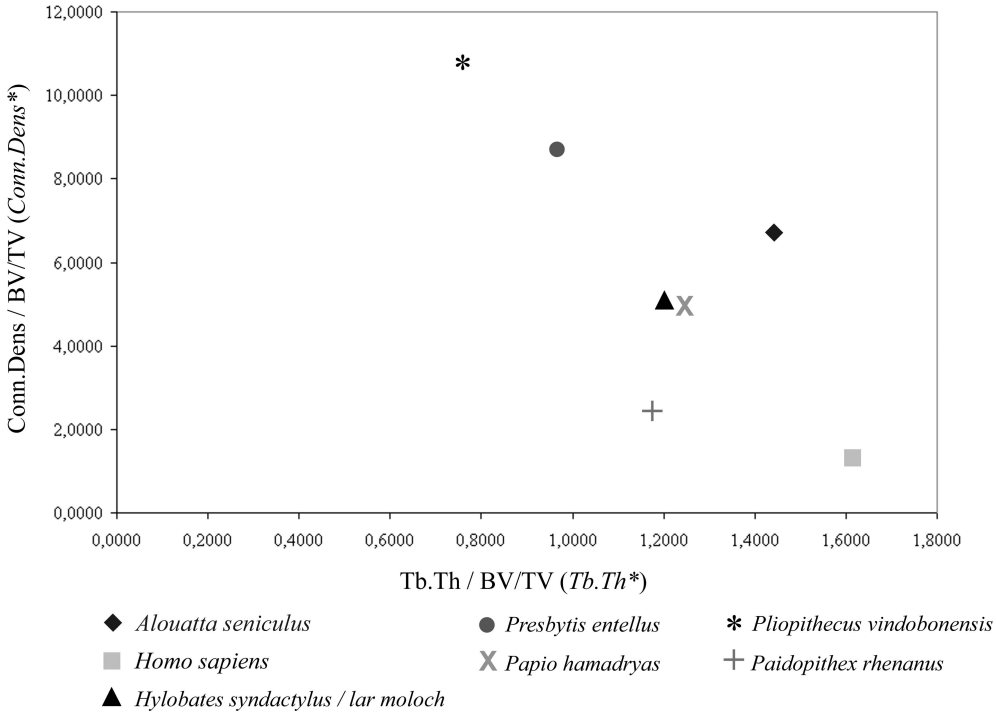

Figure 4.48: Average value Conn.D / BV/TV - Tb.Th / BV/TV

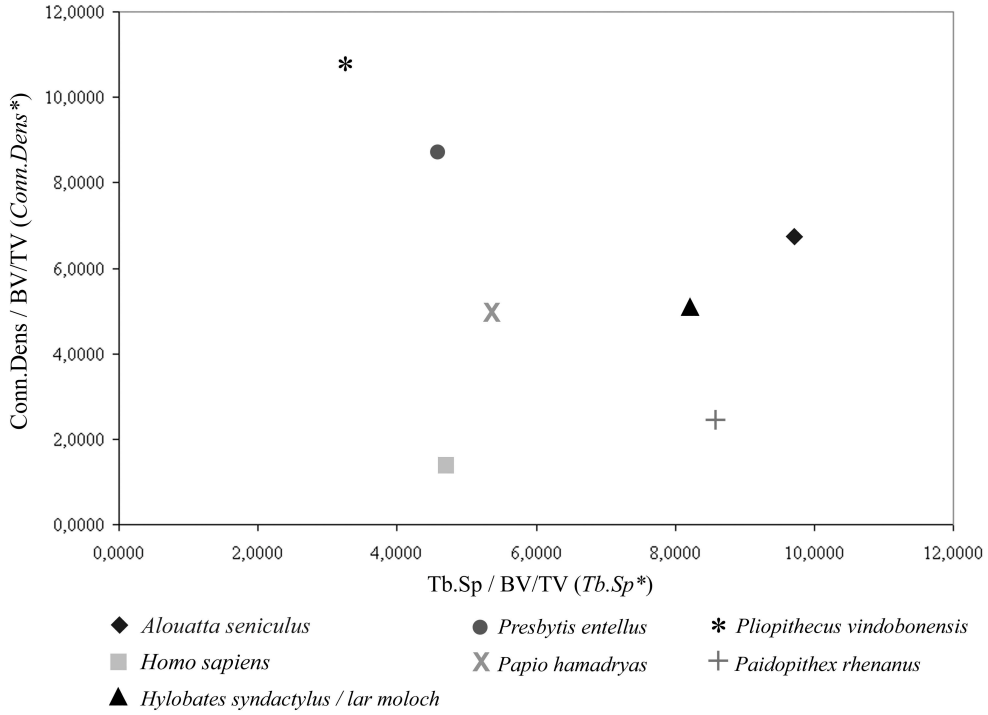

Figure 4.49: Average value Conn.D / BV/TV - Tb.Sp / BV/TV

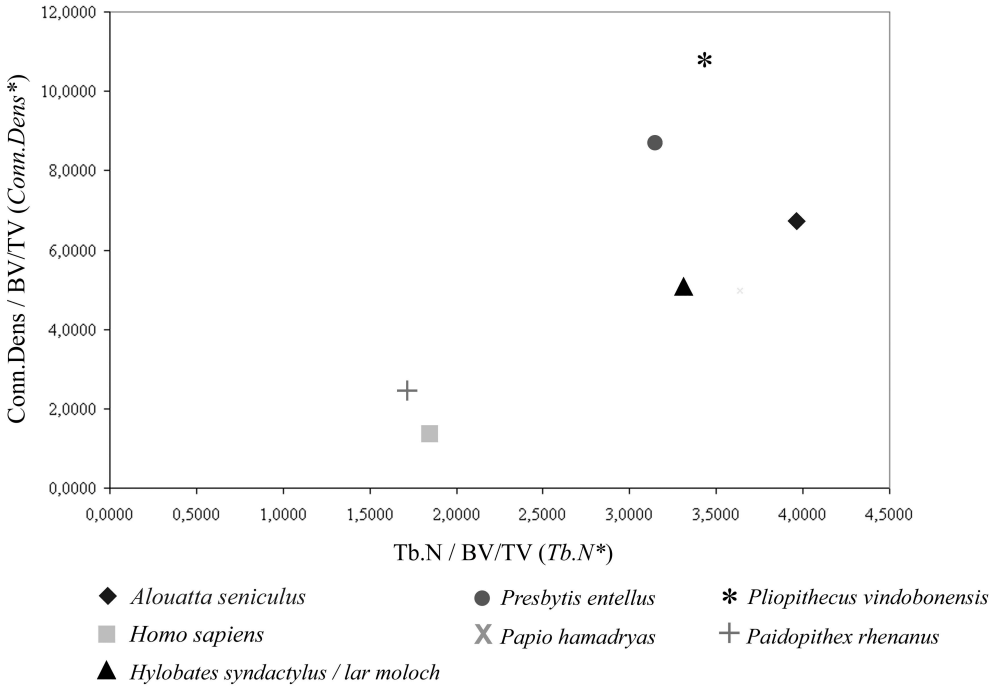

Figure 4.50: Average value Conn.D / BV/TV - Tb.N / BV/TV

The prevailing plate-like trabecular architecture in *Alouatta seniculucs* 25 544 l ♀ are reflected by an SMI of -0.1721 (Figure 4.5), while the most positive SMI in this species (69.19 l ♂; 0.5179) expresses a slightly higher abundance of rod-like and prolate elements (Figure 4.4). The same is true for *Presbytis entellus* where the high amount of large, plate-like trabeculae with some prolate or rod-like forms, is reflected by an SMI of -1.2336 at 4734 l (Figure 4.10), while the relatively higher amount of rod-like forms yield an SMI of 0.3197 at 4745 l (Figure 4.11). The ROI trabecular architecture in *Papio hamadryas* also fits with the SMI results. While HA VIII 83 l ♂ shows a high amount of large, plate-like trabeculae (SMI: -0.2664) (Figure 4.17), the size and amount of these plates decrease in HA VIII 3 l ♂ (SMI: 0.0773) (Figure 4.19) and 3212 l ♂ (SMI: 0.1007) (Figure 4.18). Finally in 1.553 l ♀ (SMI: 0.7018) prolate and rod-like elements prevail (Figure 4.20). In *Hylobates* the SMI describes a high amount of plate-like forms. The few, mainly plate-like trabecular elements in the open structure of *Hylobates lar moloch* 47 979 r ♂ contribute to an SMI of 0.0078 (Figure 4.22). However, the rather concave trabecular forms created by a denser network of mainly plate-like trabeculae in *Hylobates syndactylus* (6983 l ♂, 52.36. l ♀) (Figures 4.25, 4.26) are expressed by SMIs of -0.5846 (6983 l ♂) and -0.2553 (52.36. l ♀).

Homo sapiens show in its SMI a separation between male and female individuals. 10 l ♀, with a high amount of prolate and rod-like trabeculae, has a SMI of 0.8914 (Figure 4.34), while 22 l ♀ has a slightly higher amount of plates (SMI: 0.2707) (Figure 4.33). With negative SMIs the

two male individuals show denser trabecular networks. 21 l ♂ is composed of closely arranged plates with few connective elements as expressed by an SMI of -3.7335 (Figures 4.31, 4.32,). In *Pliopithecus vindoboensis*, only negative SMI occur, increasing from -0.2760 (1970/1397/22 r), to -0.5092 (1970/1397/23 l), then -0.7187 (O.E. 304 r), to -0.7415 (1970/1398/2 l) and -1.1061 (O.E. 559 l). This increase corresponds with an increase of large trabecular plates having small spaces and connective elements in between (Figures 4.41, 4.42, 4.43, 4.44, 4.45). *Paidopithex rhenanus* slightly exceeds the trend of *Pliopithecus vindoboensis* in showing a higher amount of closely packed plate-like trabeculae with small connecting prolate elements (SMI: -1.2845) (Figure 4.47).

The DA (Table C.1 and C.2) of *Presbytis entellus* exhibits the most anisotropic cancellous structure, while *Pliopithecus vindoboensis* has the less anisotropic DA. Both species show similar characteristics concerning the size related parameters (Figures 4.48, 4.49, 4.50). However, it must be noted that DA values vary in each species and do partly overlap between specimens of different species. The three measures of direction; minimal distance |H1|, maximal distance |H2|, and intermediate distance |H3| between the trabeculae always cover an angle of approximately 90° on all species. None of the directions |H1| - |H3| can be directly compared between the specimens as sample alignment on the CT turntable varied individually. Nonetheless, a relative comparison based on anatomical direction of the individual femora is still possible. Table 4.4 lists the direction of |H1| passing through the femora. The single components for describing spatial direction such as medial, anterior, or proximal are listed in order of decreasing influence. Directions in brackets contribute weakly to the course of |H1|.

The posterior-medial-distal to anterior-lateral-proximal direction 39.13% is the most common |H1| direction for all species. The variations medial-posterior-distal to lateral-anterior-proximal and posterior-distal-medial to anterior-proximal-lateral 17.39% are both the second most common directions. All three together (73.91%) indicate a gross common direction passing through the femur obliquely. The remaining directions are single occasions. As |H1|, |H2|, and |H3| are always at right angles to each other, their predominate directions can be derived from the direction of |H1|. Hence, |H3| passes the femora obliquely, directed in a medial-anterior-distal to lateral-posterior-proximal direction with slight individual variation in weighting of the single components. |H2| is always directed mainly in longitudinal direction with slight inclinations to the four other sides. Therefore, it seems that the main loading direction indicated by |H1|, resembling the directions with the most bone substance, is similar in all investigated specimens. The magnitude and variation of the loading conditions of the lesser trochanter seems to be rather be reflected by the size related parameters, like the Conn.Dens, the Tb.Th, the Tb.Sp, and the Tb.N, and the size independent SMI.

Table 4.4: Direction of |H1|

	from		to
Alouatta s. 69.19 l	medial-posterior-distal	→	lateral-anterior-proximal
Alouatta s. 25 544 l	anterior-medial-(distal)	→	posterior-lateral-(proximal)
Alouatta s. 25 545 l	anterior-(proximal)	→	posterior-(distal)
Presbytis e. 4734 l	posterior-distal-medial	→	anterior-proximal-lateral
Presbytis e. 4745 l	proximal-posterior-medial	→	distal-anterior-lateral
Presbytis e. 4746 l	posterior-medial-distal	→	anterior-lateral-proximal
Papio h. 1.553 l	medial-distal-(posterior)	→	lateral-proximal-(anterior)
Papio h. Ha VIII.83 l	posterior-distal-medial	→	anterior-proximal-lateral
Papio h. Ha VIII 3 l	posterior-distal-(medial)	→	anterior-proximal-(lateral)
Papio h. 3212 l	posterior-distal-medial	→	anterior-proximal-lateral
Hylobates s. 6983 l	posterior-medial-distal	→	anterior-lateral-proximal
Hylobates s. 52.36. l	medial-posterior-distal	→	lateral-anterior-proximal
Hylobates l. m. 47 979 r	posterior-medial-distal	→	anterior-lateral-proximal
Homo s. 10 l	posterior-medial-distal	→	anterior-lateral-proximal
Homo s. 11 l	posterior-medial-distal	→	anterior-lateral-proximal
Homo s. 21 l	anterior-medial-distal	→	posterior-lateral-proximal
Homo s. 22 l	posterior-medial-distal	→	anterior-lateral-proximal
Pliopithecus v. O.E. 304 r	posterior-medial-distal	→	anterior-lateral-proximal
Pliopithecus v. O.E. 559 l	medial-posterior-distal	→	lateral-anterior-proximal
Pliopithecus v. 1970/1397/22 r	posterior-medial-distal	→	anterior-lateral-proximal
Pliopithecus v. 1970/1397/23 l	posterior-medial-distal	→	anterior-lateral-proximal
Pliopithecus v. 1970/1398/2 l	medial-posterior-distal	→	lateral-anterior-proximal
Paidopithex r. Din 45 r	posterior-medial	→	anterior-lateral

4.4 FEM pilot study and consequences

In the pilot study mentioned in chapter 3.5, the trabecular architecture of the femoral trochanter minor in the extant prosimian *Lemur macaco* and the fossil prosimian *Notharctus tenebrosus* were investigated. These two species are believed to be closely related. A right femur of *Lemur macaco* was provided by the Hessische Landesmuseum Darmstadt, Germany (M-HLMD M1227). The US National Museum and Hunter College, New York, USA, provided a fragment of the proximal left femur of *Notharctus tenebrosus* (USNM 256688). Parts of the lesser and third trochanter are lacking on this fragment.

Both specimens were previously investigated regarding their trabecular architecture by Scherf et al. (2005). In this study, questions regarding the locomotor preference of *Notharctus tenebrosus* could not be settled. It is believed that both species practised a similar mode of locomotion (Gregory 1920, Szalay & Delson 1979, Fleagle 1988). Therefore, another goal of this analysis was to determine whether the locomotor loading of the femur of *Notharctus tenebrosus* was comparable to *Lemur macaco*.

The *Notharctus tenebrosus* femur was recovered from the Eocene deposits of the Bridger Basin, USA and is approximately 50 Ma old. This species is attributed to the family Adapidae and subfamily Notharctinae (Szalay & Delson 1979, Conroy 1990). The genus *Notharctus* was described in detail by Gregory (1920). From its skeletal morphology Gregory (1920) inferred that *Notharctus* demonstrated a quadrupedal, leaping mode of locomotion. Judged by the femoral morphology and the assumed arrangement of the musculature, he described a Lemur-like movement of *Notharctus* hindlimbs and further concluded that it generated a smaller leaping force than *Lemur sp.* Szalay & Delson (1979) interpreted these Eocene primates as "...limber and agile arborealists, grasp-leapers, capable of long leaps, probably occasionally practising leaping and vertical grasp clinging, and generally rapid locomotion among larger branches of the forest canopy." (page 116). Fleagle (1988) characterized *Notharctus* as a skilful leaper and quadrupedal runner but doubted the practise of vertical clinging. He also estimated that *Notharctus tenebrosus* had a body weight of approximately 4.2 kg.

Lemur macaco lives in dense forests of northwestern Madagascar and the Comoro Islands. Its arboreal way of life is associated with very agile locomotion. Quadrupedal climbing, walking or running upon horizontal and oblique branches, and maximum leaps of 8 m have been observed (Kolar 1988, Nowak 1991). Predominately they walk or run quadrupedally and occasionally cover short distances by running bipedally (Nowak 1991). The body weight of *Lemur macaco* ranges from 2-3 kg (Kolar 1988). As no information about the body weight of the sampled individual is available, a mean weight of 2.5 kg was estimated.

The loads/forces to be virtually applied on the object are crucial for FE modelling. As data about the ground reaction forces of *Lemur macaco* are not available, corresponding data of *Lemur catta*, a prosimian of comparable size and similar locomotor repertoire were used (Günther 1989). Günther (1989) measured the take-off forces of a 2.4 kg *Lemur catta* with

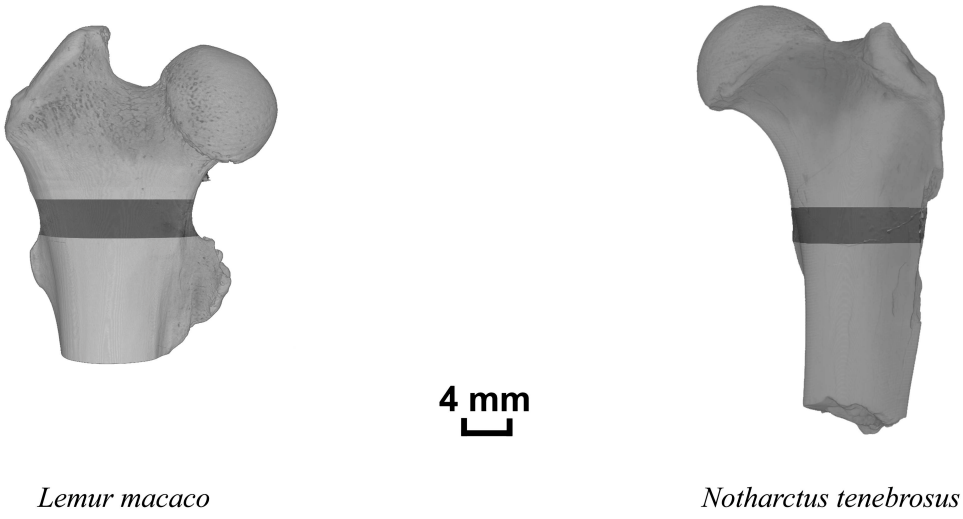

Figure 4.51: Defined regions of interest (ROI) at *Lemur macaco* and *Notharctus tenebrosus*

the peak forces being 4.3 times the body weight. *Lemur catta* spends much time on the ground walking and running (Nowak 1991), while *Lemur macaco* is characterized as a very good leaper (Kolar 1988). The peak ground reaction force was therefore roughly estimated to be 5 times body weight. The peak ground reaction force of *Notharctus tenebrosus* was assumed to be 5 times body weight as well. If *Notharctus tenebrosus* had a lesser leaping ability compared to *Lemur macaco* (Gregory 1920), a peak force 5 times the body weight should cause significantly higher stresses in its trabecular architecture.

Both specimens were CT imaged with the RayScan 200 as described in chapter 3.3. The proximal part of the *Lemur macaco* femur was scanned to a resolution of 0.029 mm. For *Notharctus tenebrosus* a resolution of 0.028 mm was obtained. All preprocessing operations such as defining a region of interest (ROI) and segmentation were accomplished with the software system VGStudio MAX. Here the ROI comprises the proximal area of the lesser trochanter. This region was chosen in accordance with the ROI of the main sample group. The locations of the ROI were defined visually. Care was taken that the ROI covered corresponding morphological regions on both specimens. On *Lemur macaco* a volume of 101 slices (2.929 mm) and on *Notharctus tenebrosus* a volume of 105 slices (2.94 mm) was selected (Figure 4.51). The ROI differ slightly between the two specimens due to differences in bone shape and damage of the lesser trochanter and the lack of a third trochanter on *Notharctus tenebrosus*.

After imaging the mineral filling of the fossil sample had to be segmented and removed virtually. Contrast in the high resolution CT slices enabled visual differentiation between filling-in and fossil bone substance. Despite good contrast automated segmentation was hindered by overlapping grey-value ranges of filling-in areas and adjoining bone regions. Therefore individual

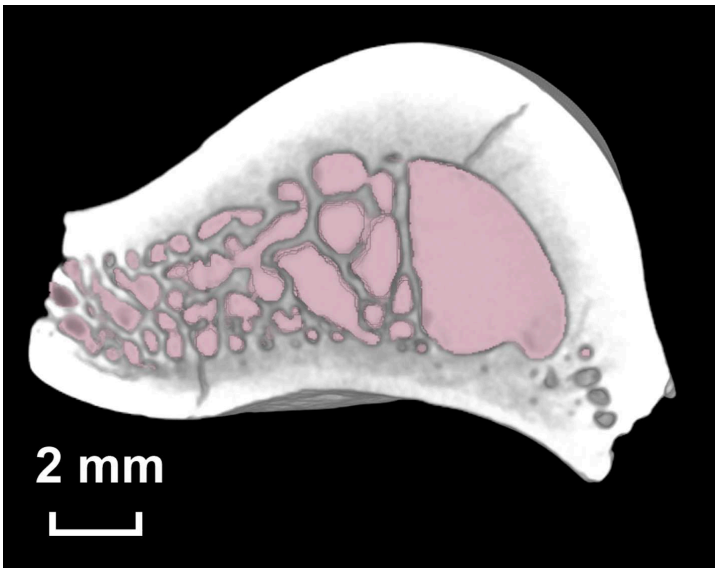

Figure 4.52: Axial view on the ROI of *Notharctus tenebrosus* with manually segmented filling-in in pink

segmentation by manual operations on each slice were made (Figure 4.52). For more consistent grey values of fossil bone and mineral filling material, respectively, the ROI was subjected to a 3x3x3 median filter. A closer examination of the *Notharctus tenebrosus* femur fragment revealed that it was imaged in a slightly oblique direction compared to the alignment of the *Lemur macaco* 3D CT image. The following operations demonstrate the importance of a consistent alignment of the specimens during the imaging procedure to reduce failure due to postprocessing operations. The *Notharctus tenebrosus* 3D CT image had to be reoriented to bring the shaft axis of its ROI in a perpendicular position. The ROI was rotated about 9.8° in vertical direction (z-direction). This operation caused a slight shift in the grey values, so that some parts of the filling-in which were left over by the former segmentation and became suppressed by a definite threshold, were now above this threshold. With a twofold processing of the 'Apply LUT' filter, all grey values were drawn below an arbitrary threshold and subsequent manual segmentation removed the final parts of the filling material. Some trabeculae became disjointed during the reorientation operation and these disconnected structures are reconstructed with the graphic tool VGStudio MAX. During reconstruction the trabeculae of the processed ROI slices were always compared with trabeculae in the unprocessed ROI data set. Afterwards the image was binarized with the 'Apply LUT' filter. All fossil bone regions were in this manner set to the maximum grey value and the surrounding area was set to a grey value of 0. The ROI of *Lemur macaco* was binarised in the same way. On the basis of the binarised images the FE models were generated.

It turned out that the data size of the FE models were too large to enable FE modelling. The model of *Lemur macaco* was made up 15 812 560 voxels while the *Notharctus tenebrosus* model was composed of 12 269 250 voxels. Data size limitation is a common problem in FE modelling of bone structures when using high volume data like high resolution CT. By virtual reduction of CT data resolution a reduction of the data size can be achieved. This reduction

is accomplished primarily by the skipping of voxels. The remaining voxels increase in size and in this way the resolution is reduced. Such operations can introduce a source of error as fine structures may be erased or thickened. However, as the given modelling limitations made a reduction in data size essential, the failures which arise through this method are also evaluated. Therefore, the final ROI data sets of *Lemur macaco* and *Notharctus tenebrosus* were reduced by a twofold and threefold skipping operation in all three dimensions. The twofold and threefold skipped data set of *Lemur macaco* has 462 198 voxels and 197 025 voxels, respectively. The *Notharctus tenebrosus* model was composed of 452 200 voxels after twofold skipping and 188 292 voxels after threefold skipping.

To evaluate how variations in loading direction influences the stress in the bone structure, the models were loaded from different directions. The load was always applied on to the proximal surface of the models while the undersurface was held rigid. First the load was rotated around the transverse axis. Therefore, it was rotated nearly 90° anteriorly and posteriorly (Direction 1) from an original perpendicular position. Subsequently the load was rotated analogously around the sagittal axis in medial and lateral direction (Direction 2). For the FE modelling an E-Modulus of 3.81 GPa and a Poisson's ratio of 0.12 was used per Jensen et al. (1990) and Wirtz et al. (2000).

The results of the FE modelling showed definite stress minima (Figures 4.53, 4.54). The position of these minima and the stress curves at the different skipping levels were somewhat similar at *Lemur macaco* while they showed differences in *Notharctus tenebrosus* especially in direction 1 (Figure 4.53). The course of these curves could be related to the locomotor behavior of the specimens. The minima may therefore correspond with architectonic features in cancellous bone which enable the directional transmission of higher loads. For a correct interpretation of the relationship between modelled stresses in trabecular architecture and locomotor behavior, the loading situation in the original structure must be deducible. However, a comparison of stress curves for the two skipping levels revealed no definite trend at both specimens.

To determine the detailed effect of the data size reduction by skipping, test cubes were extracted out of the original ROI data sets. The size of these test cubes were chosen to enable FE modelling with the original resolution. These cubes were subsequently submitted to a single skipping and twofold skipping. In this way three data sets for each specimen in three different types of decreasing resolution were gained (original, 1fold skipped, 2fold skipped). FE models were generated from these cubes and submitted to the same loading process described above. The results of the test cubes give no indication about linear interdependence between resolution, skipping levels, and the path of the stress curves (Figures 4.55, 4.56, 4.57, 4.58). It seems instead that, independent of the skipping level, any kind of original resolution alteration to reduce data size changes the path of the stress curve in a significant way. Therefore, it seems inadvisable to infer the path of the stress curves of original data from those of skipped data. Optimal results in FE modelling of loading conditions in trabecular architecture may therefore best be gained by taking the original data.

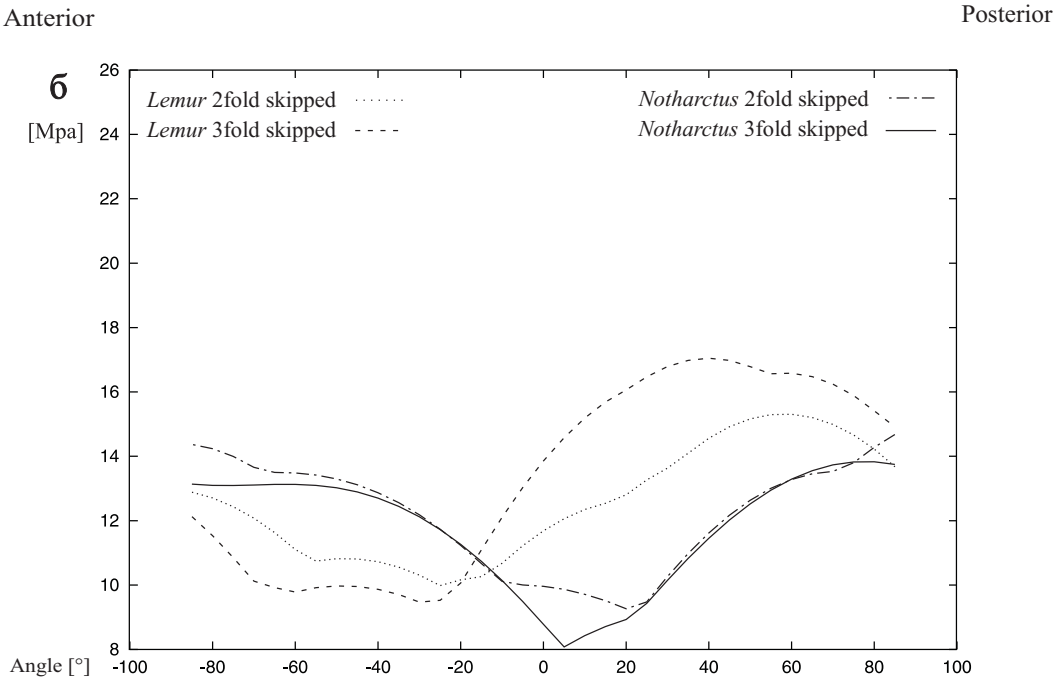

Figure 4.53: Stress curves in *Lemur macaco* and *Notharctus tenebrosus* in Direction 1

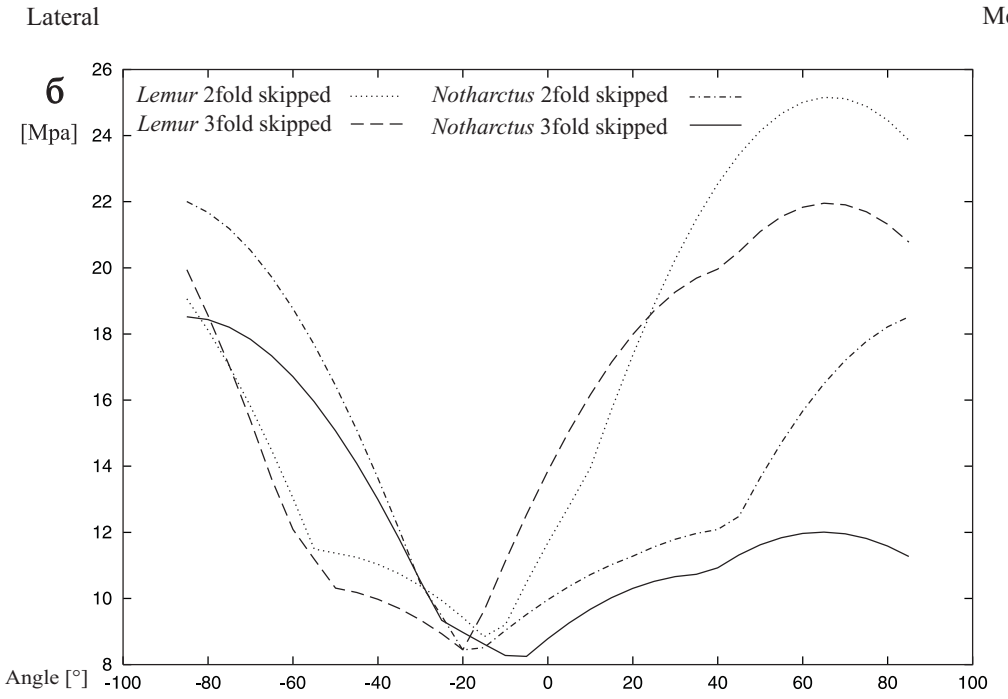

Figure 4.54: Stress curves in *Lemur macaco* and *Notharctus tenebrosus* in Direction 2

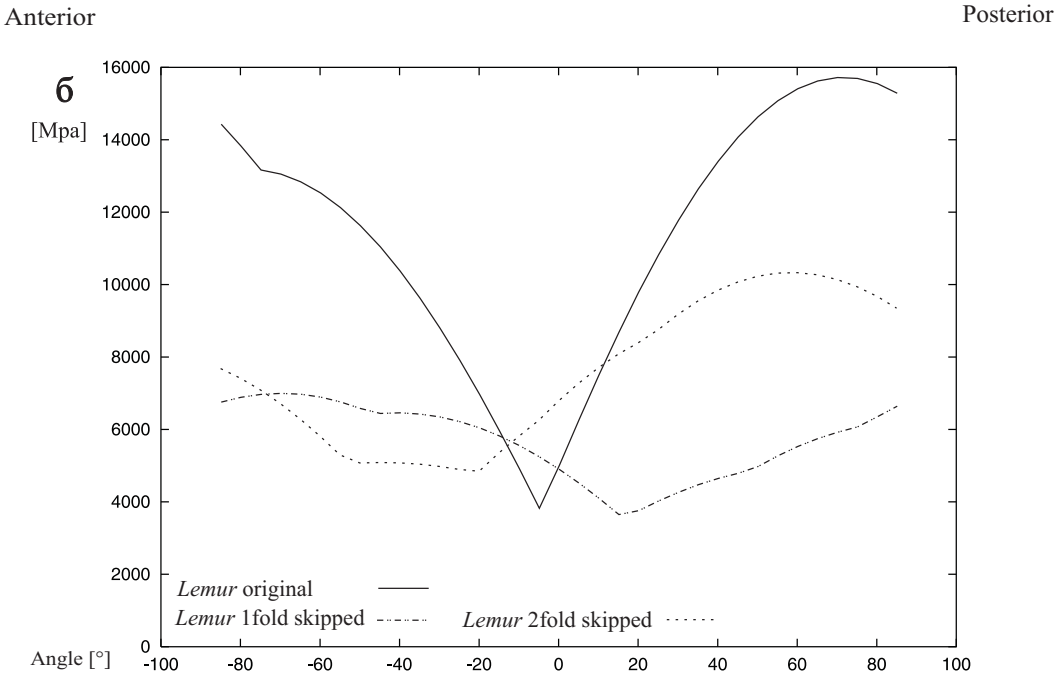

Figure 4.55: Stress curves of the test cube in *Lemur macaco* in Direction 1

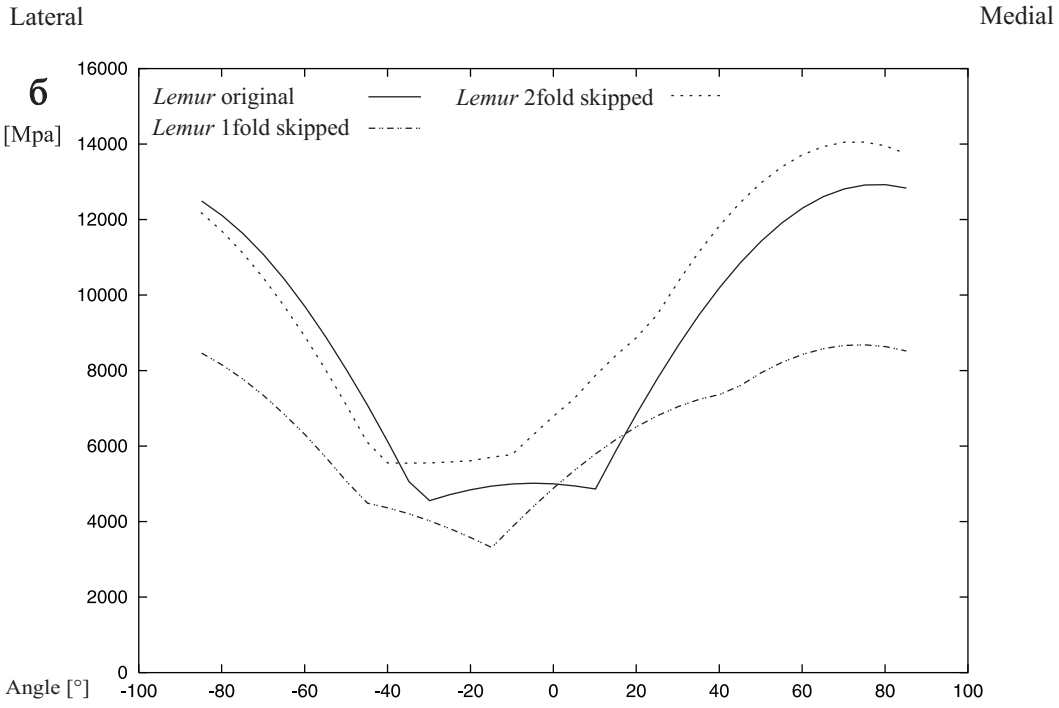

Figure 4.56: Stress curves of the test cube in *Lemur macaco* in Direction 2

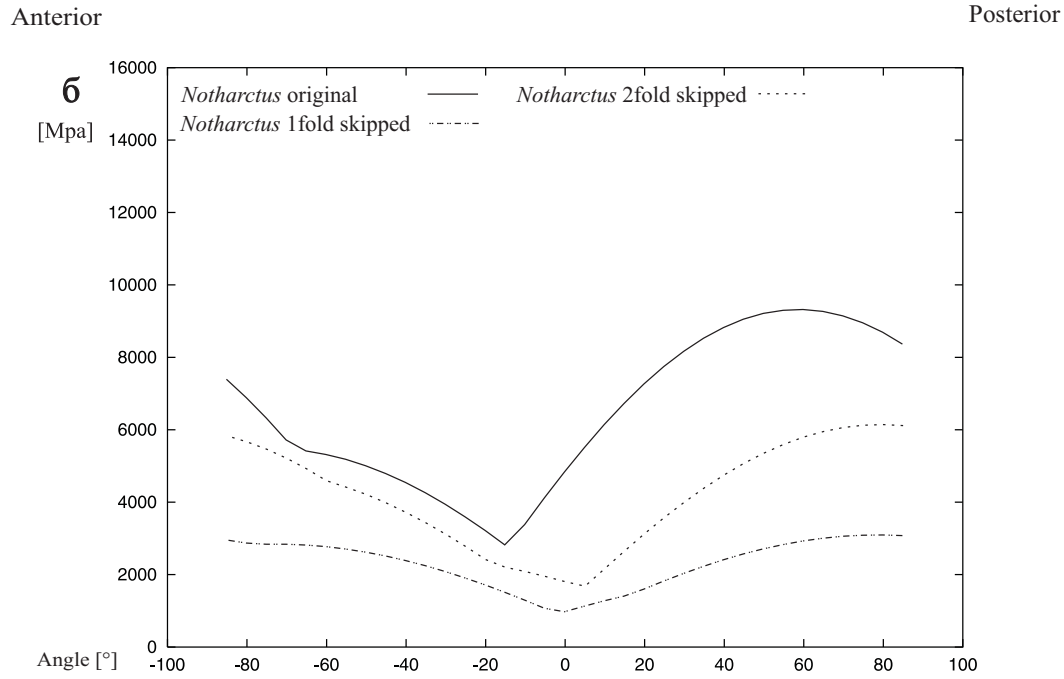

Figure 4.57: Stress curves of the test cube in *Notharctus tenebrosus* in Direction 1

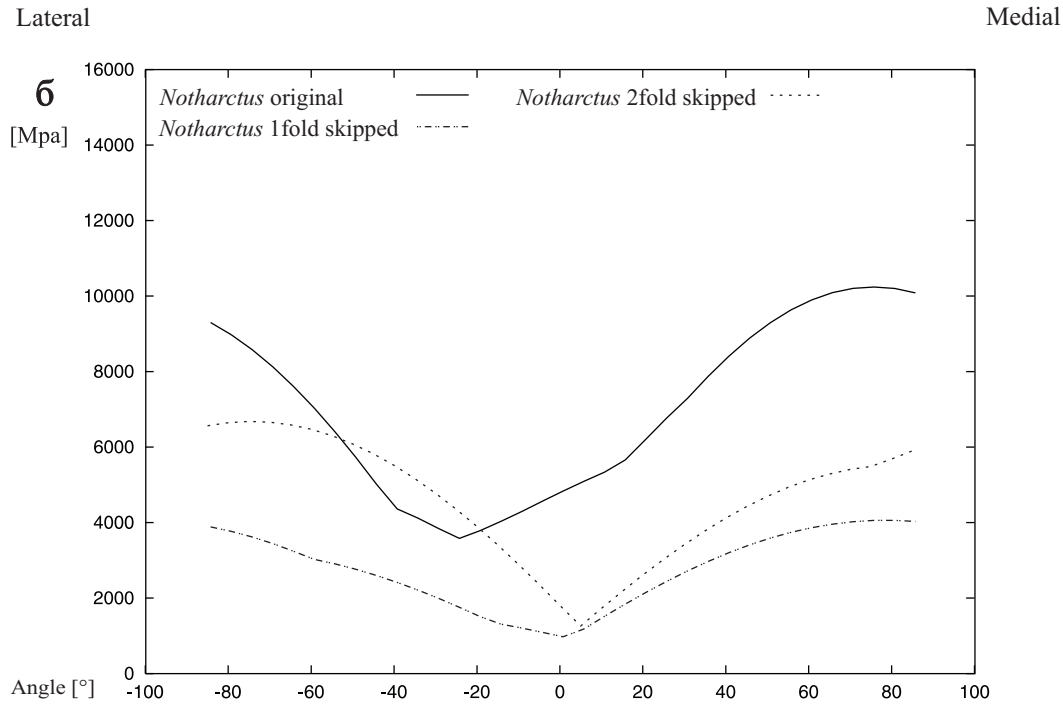

Figure 4.58: Stress curves of the test cube in *Notharctus tenebrosus* in Direction 2